Chapter 4

Multiple Effect Evaporation

Objectives

The main objective of this chapter is to evaluate the performance of the multiple effect evaporation desalination processes. This is achieved through discussion of the following:

- Process developments.
- Mathematical models and case studies.
- Detailed models and system performance.

4.1 Developments in Multiple Effect Evaporation

The multiple effect evaporation system is formed a sequence of single effect evaporators, where the vapor formed in one effect is used in the next effect. The vapor reuse in the multiple effect system allows reduction of the brine and the temperature to low values and prevent rejection of large amount of energy to the surrounding, which was the main drawback of the single effect system. In addition to the desalination industry, the main bulk of the multiple effect evaporation processes is found in the food, pulp and paper, petroleum, and petrochemical industries. As discussed in chapter 1 the origins of the multiple effect evaporation dates back to the 19^{th} century with the growth of the sugar industry, where it was necessary to devise an efficient evaporation process to produce good quality sugar crystal at low prices.

Although, the first desalination plants were of the evaporation type their use was not expanded to full industrial scale because of limited design and operating experience. Such systems were plagued with excessive fouling, scaling, and corrosion. However, accumulated experiences during the 2^{nd} half of the past century in thermal desalination processes, headed by the MSF process, have resulted in rapid progress and development of efficient and inexpensive chemical treatment for reduction and prevention of fouling, scaling, and corrosion. Such advances made it possible to maintain plant factors as high as 90% and to keep plants on-line for more than 2 years of operation. As a result, recent research, development, pilot plant operation, and field results show superior performance and the many attractive features of the multiple effect evaporation in comparison with the predominant MSF process.

The multiple effect evaporation process can be configured in forward, backward, or parallel feed, Fig. 1. The three configurations differ in the flow directions of the heating-steam and the evaporating brine. Selection among the three configurations relies on variation in the salt solubility as a function of the top brine temperature and the maximum brine concentration. At higher temperatures or higher brine concentrations, scale formation takes place inside and outside the tube surfaces. This results in the following:

- Decrease of the available flow area inside the tubes, which causes increase in the pressure drop and pumping energy, and
- Increase of the thermal resistance for heat transfer. This reduces the heat transfer efficiency, which results in a lower product flow rate.

Figure 2 shows variation in the solubility of calcium sulfate as a function of concentration and temperature. The diagrams illustrate solubility limits of calcium sulfate compounds as well as variations in the temperature-concentration profiles in the three MEE configurations. These profiles are given for the seawater and brine during their flow in the system preheaters and evaporators.

In the backward feed, the seawater is introduced into the last effect, which has the lowest temperature and pressure within the system. The brine flows through successive effects towards the first effect. The increase in the pressure and temperature across the effects dictates the use of brine pumping units between the effects.

This feature is a major disadvantage in the backward system; because of the increase in the pumping power, maintenance cost, and the increase in air leakage point through pump connections. The second disadvantage of the system is shown on Fig. 2c, where the brine with the highest concentration is subjected to the highest temperature in the system. As is shown, the temperature-concentration profile crosses the solubility limits for the calcium sulfate. The above two factors make the backward feed configuration inapplicable to seawater desalination.

Some examples for industrial applications of the parallel feed MEE can be found in literature, Temstet et al. (1995) and Temstet et al. (1996). Figures 1c shows a system schematic and Figs. 2a and 2b show the temperature-concentration profile in the parallel feed system. In this configuration, the feed seawater is divided into a set of parallel streams, which are fed into individual effects. In each effect the feed seawater is heated to the effect saturation temperature, before evaporation commences. The main advantage of the parallel feed configuration is the simplicity of its configuration in comparison with the other two layouts.

The main feature of the forward feed system is the ability to operate at high top brine temperatures, El-Dessouky et al. (1998). Detailed evaluation of this system is given in the next sections.

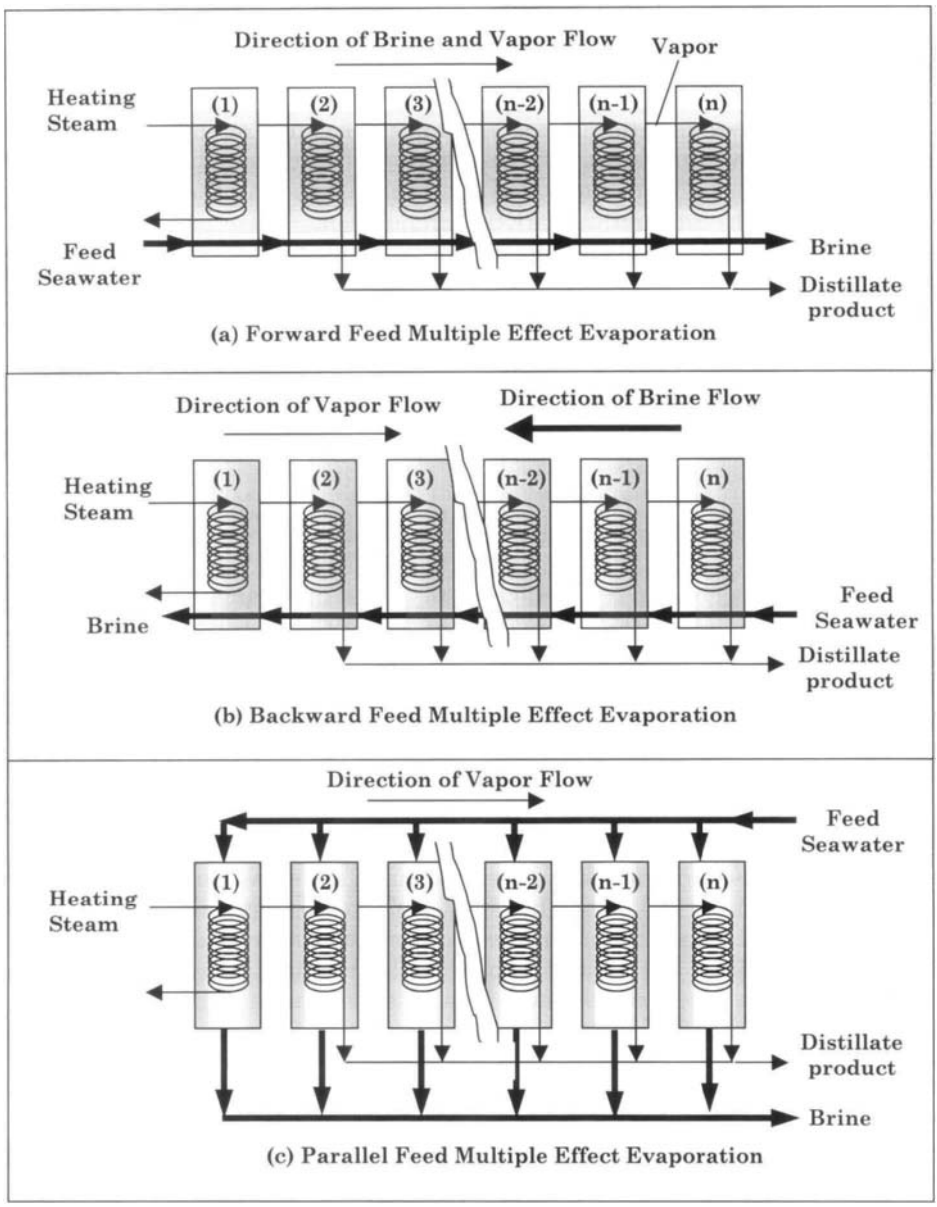

Fig. 1. Configurations of Multiple Effect Evaporation

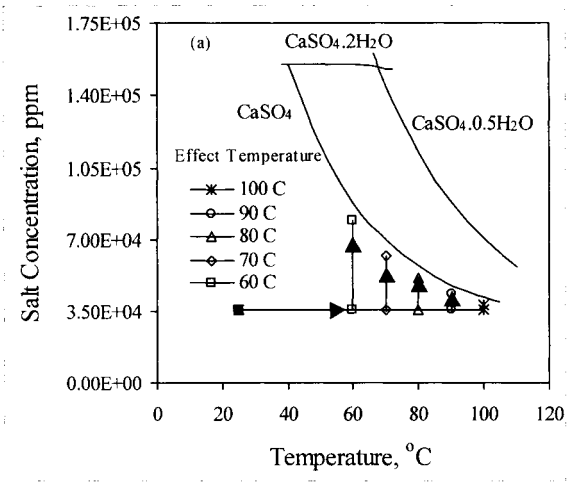

Fig. 2a. Calcium sulfate solubility and top brine temperature for parallel feed multiple effect evaporation.

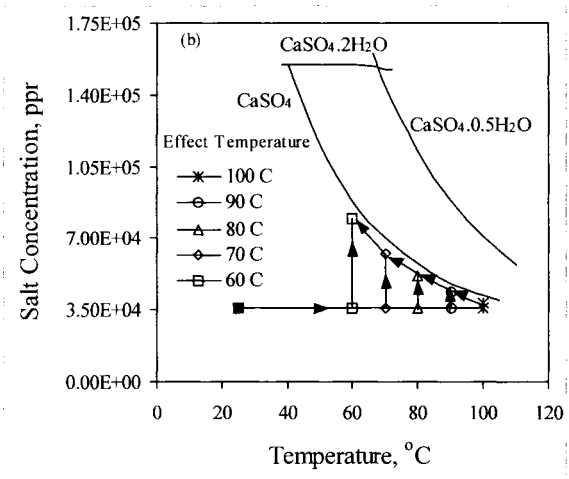

Fig. 2b. Calcium sulfate solubility and top brine temperature for parallel/cross flow multiple effect evaporation.

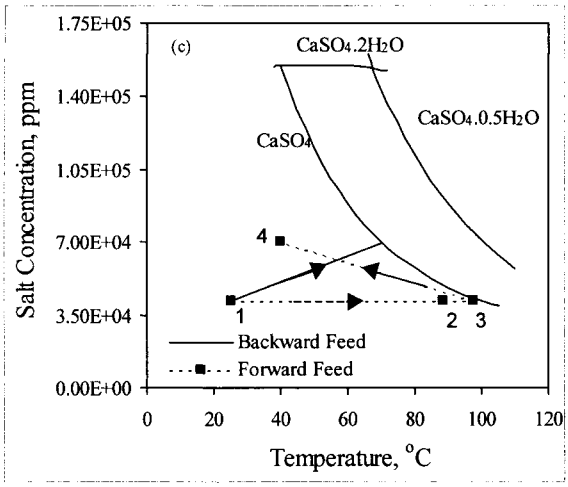

Fig. 2. Calcium sulfate solubility and top brine temperature for forward and backward feed multiple effect evaporation.

4.2 Forward Feed Multiple Effect Evaporation

Although the forward feed multiple effect evaporation system is not found on industrial scale for the desalination industry, it is widely used in the sugar and paper industries. The forward feed configuration was not used in the desalination industry because it has a more complex layout than the parallel feed configuration. In addition, the first multiple effect that were designed and constructed were of the parallel type. Field results of the parallel effect units proved their reliability; therefore, subsequent units remained to be of this design.

4.2.1 Process Description

Figure 3 shows a schematic diagram for the forward-feed Multiple-Effect Evaporation (MEE-FF) seawater desalination process. The system includes the evaporators, equal to n, a series of feed water preheaters, equal to n-2, a train of flashing boxes, equal to n-1, a down condenser, and a venting system. In the forward-feed configuration, the direction of heat flow as well as the flow direction of the brine and vapor is from left to right, i.e., from effect 1 to effect n. The pressure in the effects decreases in the flow direction. Each effect contains heat exchange tubes, vapor space, brine spray nozzles, mist eliminator, and brine collecting box. The horizontal falling film evaporator is the most widely used in the MEE desalination processes. The advantages of the horizontal falling film system are:

- Efficient water distribution and tube wetting,
- High heat-transfer rates,
- Absence of dry patches,
- Low scale formation and tube damage,
- Efficient disengagement of vapors and non-condensable gases,
- Proper venting of the non-condensable gases, and
- Simple monitoring of scaling and fouling.

The main drawback of the horizontal falling film MEE is scale and fouling on the outer surface of the tubes. This does not allow for the use of ball cleaning system, common in seawater internal flow. Such system proved to reduce internal scaling and fouling by 50% of the design value, Rautenbach and Schafer, 1997.

The intake seawater flows into the condenser of the last effect at a flow rate of $M_{cw}+M_f$. This stream absorbs the latent heat of vapors formed in the last effect and flashing box. The seawater stream is heated from the intake temperature, T_{cw}, to a higher temperature, T_f. The function of the cooling seawater, M_{cw}, is to remove the excess heat added to the system in the first effect by the motive steam. In the last effect, this heat is equivalent to the latent heat of the boiled off vapors. On the other hand, the feed seawater, M_f, is heated by the flashed off vapors formed in the last effect and the associated water flash box. The cooling seawater, M_{cw}, is rejected back to the sea. The feed seawater, M_f, is chemically treated, deaerated, and pumped through a series of preheaters. The temperature of the feed water increases from T_f to t_2 as it flows inside the tubes of the preheaters. Heating of the feed seawater is made by condensing the flashed off vapors from the effects, d_j, and the flash boxes, $\bar{d}_j$. The feed water, M_f, leaves the last preheater (associated with the second effect) and is sprayed inside the first effect. It is interesting to not that the preheater of the first effect is integrated in the heat exchanger of the effect. This is because there is no flash box in the first effect or flashed off vapors within the effect. The brine spray forms a thin film around the succeeding rows of horizontal tubes. The brine temperature rises to the boiling temperature, T_1, which corresponds to the pressure of the vapor space. The saturation temperature of the formed vapor, T_{v1}, is less than the brine boiling temperature by the boiling point elevation, $(BPE)_1$.

A small portion of vapor, D_1, is formed by boiling in the first effect. The remaining brine, $M_f - D_1$, flows into the second effect, which operates at a lower temperature and pressure. Vapor is formed in effects 2 to n by two different mechanisms, boiling and flashing. The amount vapor formed by boiling is D_j and

the amount formed by flashing is d_j. Flashing occurs in effects 2 to n because the brine temperature flowing from the previous effect, T_{j-1}, is higher than the saturation temperature of the next effect, T_{vj}. Therefore, vapor flashing is dictated by the effect equilibrium. In effects 2 to n, the temperature of the vapor formed by flashing, T'_{vj}, is lower than the effect boiling temperature, T_j, by the boiling point elevation $(BPE)_j$ and the non-equilibrium allowance (NEA)j. In the flash boxes, a small quantity of flashing vapors, $\bar{d}_j$, is formed with a temperature equal to T''_{vj}. This temperature is lower than the vapor condensation temperature in effect j, T_{cj}, by the non-equilibrium allowance $(NEA)'_j$.

Motive steam, M_S, extracted from an external boiler drives vapor formation in the first effect. The vapor formed by boiling in the first effect, D_1, is used to drive the second effect, which operates at a lower saturation temperature, T_2. Reduction in the vapor temperature is caused by boiling point elevation, non-equilibrium allowance, and losses caused by depression in the vapor saturation pressure by frictional losses in the demister, transmission lines, and during condensation. These losses can be represented as an extra resistance to the flow of heat between condensing vapor and boiling brine. Therefore, it is necessary to increase the heat transfer area to account for these losses. The amount of vapor formed in effect j is less than the amount formed in the previous effect. This is because of the increase in the latent heat of vaporization with the decrease in the evaporation temperature.

The condenser and the brine heaters must be provided with good vents, first for purging during start-up and then for removing non-condensable gases, which may have been introduced with the feed or drawn in through leaks to the system. The presence of the non-condensable gases not only impedes the heat transfer process but also reduces the temperature at which steam condenses at the given pressure. This occurs partially because of the reduced partial pressure of vapor in a film of poorly conducting gas at the interface. To help conserve steam economy venting is usually cascaded from the steam chest of one preheater to the steam chest of the adjacent one. The effects operate above atmospheric pressure are usually vented to the atmosphere. The non-condensable gases are always saturated with vapor. The vent for the last condenser must be connected to vacuum-producing equipment to compress the non-condensable gases to atmosphere. This is usually a steam jet ejector if high-pressure steam is available. Steam jet ejectors are relatively inexpensive but also quite inefficient. Since the vacuum is maintained on the last effect, the unevaporated brine flows by itself from effect to effect and only a blow down pump is required on the last effect.

Summary of different processes that takes place in each effect, the associated flash box and feed preheater is shown in Fig. 4. As is shown the brine leaving the effect decreases by the amount of vapor formed by boiling, D_j, and by flashing, d_j. The distillate flow rate leaving the flash box increases by the amount of condensing vapors from the previous effect, D_{j-1} and d_{j-1}. The brine concentration increases from X_{j-1} to X_j upon vapor formation. The effect and flash box temperatures decrease from T_{j-1} to T_j and from T'_{j-1} to T'_j, respectively.

Comparison of the process layout for MSF and MEE, show that MSF is a special case of the MEE process. This occurs when the entire vapor formed in the effects is used to preheat the feed in the preheaters and non-is left for the evaporator tubes. In this case, the first effect, the flashing boxes, and the bottom condenser of the MEE replace the brine heater, the distillate collecting trays, and the heat rejection section of the MSF, respectively.

4.2.2 Process Modeling

Two models are presented in this section. The first is the simplified mathematical model, which gives a very efficient and simple tool for system design and evaluation. The model is solved through a simple sequence of manual calculations. Iterations are not exhaustive and do not require computer programming. Also, the assumptions invoked in model development do not sacrifice process fundamentals, specifically, equal heat transfer area in all effects.

The data generated by the model is limited to the following effect properties:
- Brine and distillate flow rates.
- Brine concentration.
- Temperature.
- Heat transfer area.

The model equations exclude the flash boxes and preheaters. The governing equation for the down condenser can be included and its solution is made upon completion of the effect iterations. The following assumptions are made to develop the MEE-FF simplified model:
- Constant specific heat, Cp, for the seawater at different temperature and concentration.
- Constant thermodynamic losses in all effects.
- Constant heat transfer area in all effects.
- No vapor flashing takes place inside the effects.
- Feed seawater is at the saturation temperature of the first effect.
- Equal thermal loads in all effects.

- The formed vapors are salt free.
- The driving force for heat transfer in the effect is equal to the difference of the condensation and evaporation temperatures.
- Energy losses to the surroundings are negligible.

Taking these assumptions into consideration, the mathematical model is developed below. The number of material and energy balance equations, which can be written for each effect, is three. This assumes that the seawater is modeled as a binary mixture of fresh water and salt. In addition, there are n equation for the heat transfer rate in each effect, which relates the effect thermal load to the area, overall heat transfer coefficient, and temperature driving force. Therefore, a total of 4xn equations are used to obtain the profiles of the flow rates, concentration, and temperature across the effects as well as the heat transfer area. The unknown values are as follow:

Brine flow rates, B_1, B_2, ..., B_{n-1}, B_n	(n unknown)
Brine concentration, X_1, X_2, ... , X_{n-1}	(n-1 unknown)
Distillate flow rate, D_1, D_2, ..., D_{n-1}, D_n	(n unknown)
Effect temperature, T_1, T_2, ..., T_{n-1}	(n-1 unknown)
Steam flow rate	(1 unknown)
Heat transfer area	(1 unknown)
	Total = (4 n) unknowns

Solution of the model equations to determine the variables, requires specification of the following system parameters:

- Temperature of the motive steam, T_s.
- Vapor temperature in effect n, T_n.
- Salt concentration in the brine stream leaving effect n, X_n.
- Salt concentration in the feed stream, X_f.
- Total distillate flow rate, M_d.

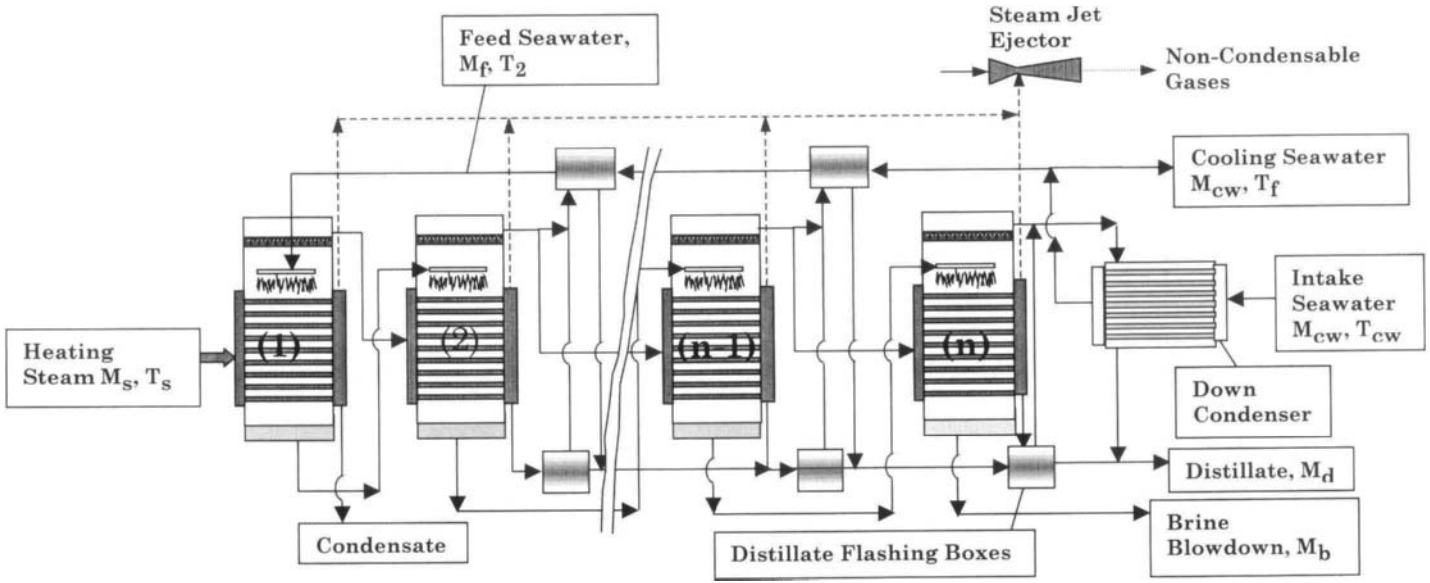

Fig. 3. Schematic of MEE-FF desalination process

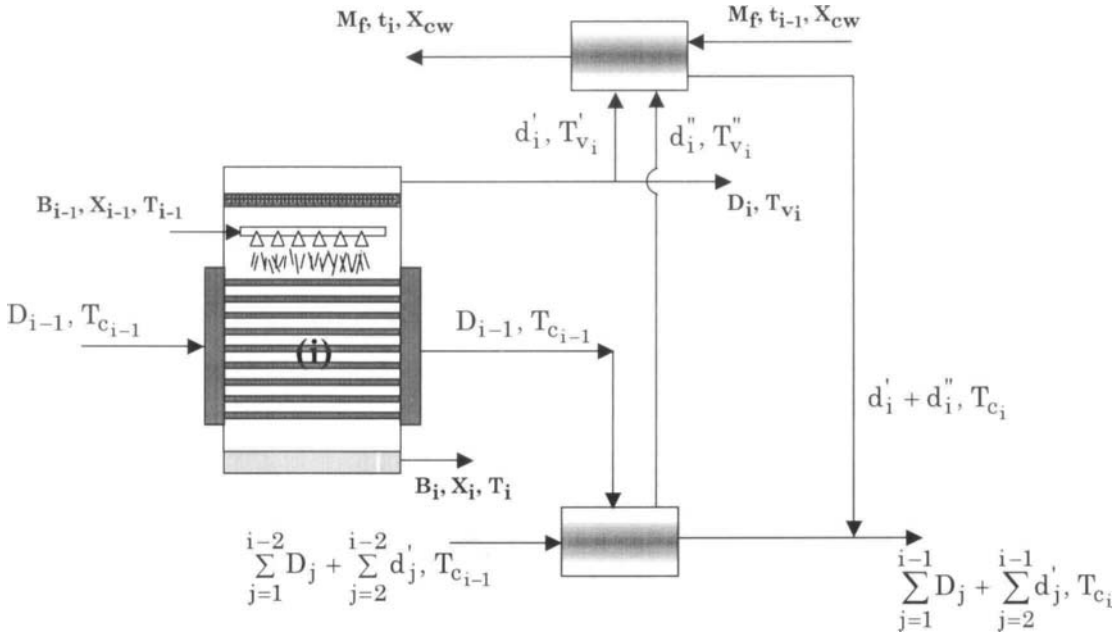

Fig. 4. Variables in evaporator, preheater, and flash box of effect i.

The overall material and salt balance equations are written to determine the brine flow rate leaving effect n, B_n, and the feed flow rate, M_f. These equations are

$$M_f = M_d + B_n \quad (1)$$

$$X_f M_f = X_n B_n \quad (2)$$

Substituting 1 in 2 and eliminating M_f gives

$$B_n = (X_f / (X_n - X_f)) M_d \quad (3)$$

All variables on the right hand side of Eq. 3 are previously specified; therefore, the value of B_n can be calculated. The overall balance, Eq. 1, is then used to determine M_f. Calculations of B_n and M_f are only made once are not included in the following iteration sequence.

Temperature Profile

The thermal load in all effects is assumed constant, thus

$$Q_1 = Q_2 = \ldots = Q_{n-1} = Q_n \quad (4)$$

with

$$Q_1 = M_S \lambda_S, \text{ for the first effect} \quad (5)$$

$$Q_i = D_i \lambda_{v_i}, \text{ for effects 2 to n} \quad (6)$$

where Q is the thermal load, M_S is the mass flow rate of motive steam, D_i is the distillate flow rate in effect i, λ_S is the steam latent heat at T_S, and λ_{v_i} is the latent heat of formed vapors at $(T_i - \Delta T_{loss})$, and the subscript i, s, and v defines effect i, the steam, and the formed vapor. The thermal load in each effect can also be defined in terms of the heat transfer area in the effect, A, the temperature driving force, ΔT, and the overall heat transfer coefficient, U. This is

$$Q_i = A_i U_i \Delta T_i \quad (7)$$

Since the heat transfer area and thermal load are equal in all effects, then

$$Q_1/A_1 = Q_2/A_2 = \ldots = Q_{n-1}/A_{n-1} = Q_n/A_n \quad (8)$$

From 7 and 8, the following identity also applies

$$U_1 \Delta T_1 = U_2 \Delta T_2 = \ldots = U_{n-1} \Delta T_{n-1} = U_n \Delta T_n \quad (9)$$

The total temperature drop across the effects is defined as

$$\Delta T = T_s - T_n \quad (10)$$

where T_s and T_n are the temperatures of the motive steam and the vapor formed in the last effect, n. This drop is also equal to the sum of temperature drop per effect, or

$$\Delta T = \Delta T_1 + \Delta T_2 + \ldots + \Delta T_{n-1} + \Delta T_n \quad (11)$$

Equations 9 and 11 can be used to define ΔT_1 in terms of the overall heat transfer coefficient and the total temperature drop in all effects. From 9, ΔT_2 can be expressed in terms of ΔT_1 by

$$\Delta T_2 = \Delta T_1 U_1/U_2 \quad (12)$$

Also ΔT_3 can be expressed in terms of ΔT_2 by

$$\Delta T_3 = \Delta T_2 U_2/U_3 \quad (13)$$

Substituting 12 in 13 gives

$$\Delta T_3 = \Delta T_1 U_1/U_2 U_2/U_1$$

which simplifies to $\Delta T_3 = \Delta T_1 U_1/U_3$. The same applies for all other effects and this general relation is arrived at

$$\Delta T_i = \Delta T_1 U_1/U_i \quad (14)$$

Substituting the result given in Eq. 14 in Eq. 11 gives

$$\Delta T = \Delta T_1 U_1 (1/U_1 + 1/U_2 + \ldots + 1/U_{n-1} + 1/U_n) \quad (15)$$

Equation 15 is rearranged into the following form

$$\Delta T_1 = \frac{\Delta T_t}{U_1 \sum_{i=1}^{n} \frac{1}{U_i}} \tag{16}$$

If estimates for U_i are made, then, temperature drop in all effects can be obtained from Eqs. 16 and 14. The actual temperature profile is then calculated from the following relations. In the first effect

$$T_1 = T_s - \Delta T_1 \tag{17}$$

and in effects 2 to n

$$T_i = T_{i-1} - \Delta T_1 \, U_1/U_i \tag{18}$$

Calculation of the temperature profile from Eqs. 17 and 18 requires specification of the overall heat transfer coefficients, U_i.

Profiles of salt concentration and flow rates of brine and distillate

The distillate flow rates are obtained from the following balance and the thermal loads, Eq. 6,

$$M_d = D_1 + D_2 + \ldots\ldots + D_{i-1} + D_n \tag{19}$$

$$D_i \, \lambda_{v_i} = D_{i-1} \, \lambda_{v_{i-1}}, \text{ for effects 2 to n} \tag{20}$$

Eq. 20 is used to express the values of D_i (for i = 2 to n) in terms of D_1, where

$D_2 = D_1 \, \lambda_{v_1}/\lambda_{v_2}$, and

$D_3 = D_2 \, \lambda_{v_2}/\lambda_{v_3} = D_1 \, (\lambda_{v_1}/\lambda_{v_2}) \, (\lambda_{v_2}/\lambda_{v_3}) = D_1 \, \lambda_{v_1}/\lambda_{v_3}$

A general recursive formula is then arrived at

$$D_i = D_1 \, \lambda_{v_1}/\lambda_{v_i}, \text{ with i = 2 to n,} \tag{21}$$

Substituting Eq. 21 in Eq. 19 gives

$$M_d = D_1 + D_1 \, \lambda_{v_1}/\lambda_{v_2} + \ldots\ldots + D_1 \, \lambda_{v_1}/\lambda_{v_{n-1}} + D_1 \, \lambda_{v_1}/\lambda_{v_n} \tag{22}$$

Eq. 21 is then rearranged to obtain an expression for D_1

$$D_1 = M_d/(\lambda_{v_1}(1/\lambda_{v_1} + 1/\lambda_{v_2} + \ldots\ldots + 1/\lambda_{v_{n-1}} + 1/\lambda_{v_n})) \quad (23)$$

The recursive formula of 21 is then used to obtain the distillate flow rates in other effects

$$D_2 = D_1 \lambda_{v_1}/\lambda_{v_2}$$

$$D_3 = D_1 \lambda_{v_1}/\lambda_{v_3}$$

$$D_n = D_1 \lambda_{v_1}/\lambda_{v_n}$$

The brine flow rate in the first effect can be obtained from

$$B_1 = M_f - D_1 \quad (24)$$

In effects 2 to n, this is given by

$$B_i = B_{i-1} - Di \quad (25)$$

Similar salt balances on the first effect and effect 2 to n are written to obtain X_1 and X_2 to X_n.

$$X_1 = X_f \ M_f/B_1 \quad (26)$$

$$X_i = X_{i-1} \ B_{i-1}/B_i \quad (27)$$

Heat Transfer Area

The heat transfer areas in effects 1 to n must be calculated to check the basic assumption of the model, i.e., equal heat transfer areas. The heat transfer area in the first effect is given by

$$A_1 = \frac{D_1\lambda_{v1}}{U_1(T_s - T_1)} \quad (28)$$

and for effects 2 to n it is defined as

$$A_i = \frac{D_i\lambda_i}{U_i(T_i - \Delta T_{loss})} \quad (29)$$

The ΔT_{loss} in the above equation corresponds to the thermodynamic losses in each effect and its value may vary from 0.5-3 °C.

Convergence Criterion and Setting up for New Iteration

The convergence criterion is based on the maximum difference in the heat transfer areas. This is given by

$$\Delta A_{max} = Max(A_{i+1} - A_i), \text{ with } i = 1,n-1 \quad (30)$$

If ΔA_{max} is greater than the specified iteration tolerance then the iterations continue. The iteration tolerance may be specified as a large number, i.e., 1 m^2, if a small number of iterations (1 or 2) are needed. However, if higher accuracy is required, then a smaller tolerance is specified, i.e., 0.1 or 0.01 m^2.

If the error is higher than the tolerance, then a new estimate for ΔT_i is made

$$\Delta T'_i = \Delta T_i \, A_i/Am \quad (31)$$

where Am is the average heat transfer area and is obtained from

$$A_m = \frac{\sum_{i=1}^{n} A_i}{n} \quad (32)$$

Iterations continue by calculating

- The temperature profile, T_i, in effects 1 to n from Eqs. 17 and 19.
- The distillate flow rate in the first effect, D_1, Eq. 23.
- The distillate flow rates in effects 2 to n, D_i, Eq. 21.
- The brine flow rate in the first effect, B_1, Eq. 24.
- The brine flow rates in effects 2 to n, B_i, Eq. 25.
- The salt concentration in the first effect, X_1, Eq. 26.
- The salt concentration effects 2 to n, X_i, Eq. 27.
- The heat transfer area in effects 1 to n, A_i, Eqs. 28 and 29.

The convergence criterion, Eq. 30, is then checked and iterations continue until it is achieved. Reaching the final solution is followed by calculation of the system performance characteristics, i.e., performance ratio, specific heat transfer area, and specific cooling water flow rate.

Performance Parameters

The performance ratio, PR, is defined as the flow rate ratio of distillate (M_d) and motive steam (M_S). This is

$$PR = M_d/M_S \tag{33}$$

The value of the steam flow rate, M_S, is obtained from the assumption of equal thermal loads, where

$$M_S = D_1 \lambda_{v1}/ \lambda_S \tag{34}$$

The specific heat transfer area is

$$sA = \frac{\sum_{i=1}^{n} A_i + A_c}{M_d} \tag{35}$$

where A_i is the heat transfer area in effect i and A_c is the down condenser heat transfer area, which is obtained from

$$A_c = \frac{Q_c}{U_c (LMTD)_c} \tag{36}$$

The $(LMTD)_c$ is defined as:

$$(LMTD)_c = \frac{T_f - T_{cw}}{\ln \frac{T_n - T_{cw}}{T_n - T_f}} \tag{37}$$

where T_{cw} is the intake seawater temperature, T_f, is the outlet seawater temperature, and T_n is the condensation temperature of the vapor formed in the last effect. The thermal load of the condenser is calculated from

$$Q_c = D_n \lambda_{vn} \tag{38}$$

The specific cooling water flow rate is defined as

$$sM_{cw} = M_d/M_{cw} \tag{39}$$

where M_{cw} is the cooling water flow rate and is obtained from the condenser energy balance

$$D_n \lambda_{v_n} = (M_f + M_{cw}) Cp (T_f - T_{cw}) \quad (40)$$

It should be noted that T_f is the feed seawater temperature entering the preheater associated with effect, n-1.

Example 1:

The above model is used to determine performance of six effects MEE system. The following specifications are made to solve the simplified MEE model:
Number of effect, n = 6,
Motive steam temperature, T_s = 100 °C,
Total product flow rate, M_d = 1 kg/s,
Salt concentration in feed seawater, X_f = 42000 ppm,
Salt concentration in rejected brine, X_6 = 70000 ppm
Vapor temperature in last effect, T_6 = 40 °C.
Thermodynamic losses in all effects, ΔT_{loss} = 2 °C.
Seawater temperature leaving the condenser, T_f = 35 °C.
Intake seawater temperature, T_{cw} = 25 °C.

Before starting the iterations, the latent heat of the motive steam and the vapor formed in the last effect are obtained from the steam tables or the correlation given in Appendix A. This gives

$$\lambda_s = 2499.5698 - 2.204864\, T_s - 2.304\text{x}10^{-3}\, T_s^2$$
$$= 2499.5698 - 2.204864\,(100) - 2.304\text{x}10^{-3}\,(100)^2$$
$$= 2256.043 \text{ kJ/kg}$$

$$\lambda_{v6} = 2499.5698 - 2.204864\, T_{v6} - 2.304\text{x}10^{-3}\, T_{v6}^2$$
$$= 2499.5698 - 2.204864\,(40\text{-}2) - 2.304\text{x}10^{-3}\,(40\text{-}2)^2$$
$$= 2412.45 \text{ kJ/kg}$$

The flow rates of the brine leaving effect number 6 and the feed seawater are obtained from Eqs. 1 and 2. The brine flow rate in effect number 6 is

$$B_6 = (X_f/(X_6\text{-}X_f))\, M_d = (42000/(70000\text{-}42000))\,(1) = 1.5 \text{ kg/s}$$

Then the feed flow rate, M_f, is equal to the sum of M_d and B_6

$B_6 = 1 + 1.5 = 2.5$ kg/s

The total temperature drop across the effects, $T_S - T_6$, is equal to 100 – 40 = 60 °C. The overall heat transfer coefficients in effects 1 to 6 are specified and are assumed to remain constant throughout the iterations. The overall heat transfer coefficient in the first effect, U_1, is set equal to 2.4 kW/m^2 °C. Values in subsequent effects are obtained from

$U_{i+1} = 0.95\ U_i$

Values of the overall heat transfer coefficient in all effects are summarized in the following table

U_1	U_2	U_3	U_4	U_5	U_6
2.4	2.28	2.16	2.0577	1.9548	1.8571

The summation of the inverse for the overall heat transfer coefficients is required to calculate the temperature drop per effect. This summation is

$$\frac{1}{\sum_{i=1}^{6} U_i} = 1/U_1 + 1/U_2 + 1/U_3 + 1/U_4 + 1/U_5 + 1/U_6$$

$$= 1/2.4 + 1/2.28 + 1/2.16 + 1/2.0577 + 1/1.9548 + 1/1.8571$$

$$= 2.8529 \text{ m}^2\ ^\circ\text{C/kW}$$

The temperature drop in the first effect is then calculated

$$\Delta T_1 = \frac{\Delta T_t}{U_1 \sum_{i=1}^{n} \frac{1}{U_i}} = \frac{60}{(2.4)(2.8529)} = 8.7628\ ^\circ\text{C}$$

The values of ΔT_i are calculated for effects 2 to 6

$\Delta T_2 = \Delta T_1\ (U_1/U_2) = (8.7628)(2.4)/(2.28) = 9.224\ ^\circ$C

$\Delta T_3 = \Delta T_1\ (U_1/U_3) = (8.7628)(2.4)/(2.166) = 9.7095\ ^\circ$C

$\Delta T_4 = \Delta T_1\ (U_1/U_4) = (8.7628)(2.4)/(2.0577) = 10.2205\ ^\circ$C

$\Delta T_5 = \Delta T_1\ (U_1/U_5) = (8.7628)(2.4)/(1.9548) = 10.7584\ ^\circ$C

$\Delta T_6 = \Delta T_1 (U_1/U_6) = (8.7628)(2.4)/(1.8571) = 11.3247\ ^oC$

The following table summarizes the above values

ΔT_1	ΔT_2	ΔT_3	ΔT_4	ΔT_5	ΔT_6
8.7628	9.224	9.7095	10.2205	10.7584	11.3247

It should be noted that the temperature drop per effect increases as the effect temperature is reduced, i.e., $\Delta T_1 > \Delta T_2 > \Delta T_3 > \Delta T_4 > \Delta T_5 > \Delta T_6$. This is dictated by

- Constant heat transfer area,
- Lower overall heat transfer coefficients at lower temperatures, and
- Constant thermal loads in all effects.

Therefore, the increase of the temperature drop at lower temperatures compensates the decrease in the overall heat transfer coefficient.

The temperature profile in effects 1 to 6 is then calculated from Eqs. 17 and 18.

$T_1 = T_S - \Delta T_1 = 100 - 8.762 = 91.2372\ ^oC$

$T_2 = T_1 - \Delta T_1 (U_1/U_2) = 91.2372 - 8.762\ (2.4/2.28) = 82.0132\ ^oC$

$T_3 = T_2 - \Delta T_1 (U_1/U_3) = 82.0132 - 8.762\ (2.4/2.166) = 72.3037\ ^oC$

$T_4 = T_3 - \Delta T_1 (U_1/U_4) = 72.3037 - 8.762\ (2.4/2.28) = 62.0831\ ^oC$

$T_5 = T_4 - \Delta T_1 (U_1/U_5) = 62.0831 - 8.762\ (2.4/2.28) = 51.3247\ ^oC$

To check the above values T_6 is calculated on

$T_6 = T_5 - \Delta T_1 (U_1/U_6) = 51.3247 - 8.762\ (2.4/1.8571) = 40\ ^oC$

This value checks with the initial specification of 40 °C.

The following table includes summary of calculated temperatures as well as the temperature of the motive steam.

T_S	T_1	T_2	T_3	T_4	T_5	T_6
100	91.2	82.01	72.3	62.1	51.3	40

The latent heat values in all effects are calculated using the correlation given in Appendix A

$\lambda_{v1} = 2499.5698 - 2.204864\ T_{v1} - 2.304x10^{-3}\ T_{v1}^2$
$= 2499.5698 - 2.204864\ (91.2372-2) - 2.304x10^{-3}\ (91.2372-2)^2$
$= 2284.47$ kJ/kg

$\lambda_{v2} = 2499.5698 - 2.204864\ T_{v2} - 2.304x10^{-3}\ T_{v2}^2$
$= 2499.5698 - 2.204864\ (82.0132-2) - 2.304x10^{-3}\ (82.0132-2)^2$
$= 2308.4$ kJ/kg

$\lambda_{v3} = 2499.5698 - 2.204864\ T_{v3} - 2.304x10^{-3}\ T_{v3}^2$
$= 2499.5698 - 2.204864\ (72.3037-2) - 2.304x10^{-3}\ (72.3037-2)^2$
$= 2333.17$ kJ/kg

$\lambda_{v4} = 2499.5698 - 2.204864\ T_{v4} - 2.304x10^{-3}\ T_{v4}^2$
$= 2499.5698 - 2.204864\ (62.0831-2) - 2.304x10^{-3}\ (62.0831-2)^2$
$= 2358.78$ kJ/kg

$\lambda_{v5} = 2499.5698 - 2.204864\ Tv_5 - 2.304x10^{-3}\ Tv_5^2$
$= 2499.5698 - 2.204864\ (51.3247-2) - 2.304x10^{-3}\ (51.3247-2)^2$
$= 2385.21$ kJ/kg

The latent heat value in the effect number 6 is calculated previously, and its value is equal to 2412.46 kJ/kg. Summary of the latent heat values is given in the following table, which includes the latent heat of motive steam.

λ_s	λ_{v1}	λ_{v2}	λ_{v3}	λ_{v4}	λ_{v5}	λ_{v6}
2256.043	2284.47	2308.4	2333.17	2358.78	2385.21	2412.46

The flow rate profiles of the distillate and brine as well as the brine concentrations are calculated from Eqs. 21 and 23-27. The distillate flow rate in the first effect is calculated from Eq. 23

$D_1 = M_d /(1 + \lambda_{v1}/\lambda_{v2} + \lambda_{v1}/\lambda_{v3} + \lambda_{v1}/\lambda_{v4} + \lambda_{v1}/\lambda_{v5} + \lambda_{v1}/\lambda_{v6})$
$= (1)/(1 + (2284.47/2308.4) + (2284.47/2333.17)$
$+ (2284.47/2358.78) + (2284.47/2385.21)$
$+ (2284.47/2412.46))$
$= 0.1712$ kg/s

Subsequently, the distillate flow rates in effects 2 to n are calculated

$D_2 = D_1 \lambda_{V1}/\lambda_{V2} = 0.1712\ (2284.47/2308.4) = 0.1694$ kg/s

$D_3 = D_1 \lambda_{V1}/\lambda_{V3} = 0.1712\ (2284.47/2333.17) = 0.1676$ kg/s

$D_4 = D_1 \lambda_{V1}/\lambda_{V4} = 0.1712\ (2284.47/2358.78) = 0.1658$ kg/s

$D_5 = D_1 \lambda_{V1}/\lambda_{V5} = 0.1712\ (2284.47/2385.21) = 0.1639$ kg/s

$D_6 = D_1 \lambda_{V1}/\lambda_{V6} = 0.1712\ (2284.47/2412.46) = 0.1621$ kg/s

The brine flow rates are obtained from Eqs. 24 and 25

$B_1 = M_f - D_1 = 2.5 - 0.1712 = 2.3288$ kg/s

$B_2 = B_1 - D_2 = 2.3288 - 0.1694 = 2.1594$ kg/s

$B_3 = B_2 - D_3 = 2.1594 - 0.1676 = 1.9918$ kg/s

$B_4 = B_3 - D_4 = 1.9918 - 0.1658 = 1.826$ kg/s

$B_5 = B_4 - D_5 = 1.826 - 0.1639 = 1.6621$ kg/s

The above calculations are checked by determining the value of B_6

$B_6 = B_5 - D_6 = 1.6621 - 0.1621 = 1.5$ kg/s

This value checks with the initial material balance calculations. The salt concentration profile is calculated from Eqs. 26 and 27.

$X_1 = X_f M_f / B_1 = 42000\ (2.5/2.3288) = 45087.6$ ppm

$X_2 = X_1 B_1/B_2 = 45087.6\ (2.3288/2.1594) = 48625$ ppm

$X_3 = X_2 B_2/B_3 = 48625\ (2.1594/1.9918) = 52716.8$ ppm

$X_4 = X_3 B_3/B_4 = 52716.8\ (1.9918/1.826) = 57502.8$ ppm

$X_5 = X_4 B_4/B_5 = 57502.8\ (1.826/1.6621) = 63174.3$ ppm

The value of X_6 is specified in the problem statement at 70,000 ppm. Summary for the values of distillate and brine flow rates and brine concentration are given in the following table.

Effect	1	2	3	4	5	6
D (kg/s)	0.1712	0.1694	0.1676	0.1658	0.1639	0.1621
B (kg/s)	2.3288	2.1594	1.9918	1.826	1.6621	1.5
X (ppm)	45087.6	48625	52716.8	57502.8	63174.3	70000

The heat transfer areas are calculated in effects 1 to 6. These values are

$$A_1 = D_1 \lambda_{v_1}/(U_1(T_s - T_1)) = (0.1712)(2284.47)/(2.4(100 - 91.24))$$
$$= 18.59 \text{ m}^2$$

$$A_2 = D_2 \lambda_{v_2}/(U_2(\Delta T_2 - \Delta T_{loss})) = (0.1694)(2308.4)/(2.28(9.224-2))$$
$$= 23.74 \text{ m}^2$$

$$A_3 = D_3 \lambda_{v_3}/(U_3(\Delta T_3 - \Delta T_{loss})) = (0.1676)(2333.17)/(2.166(9.7095-2))$$
$$= 23.41 \text{ m}^2$$

$$A_4 = D_4 \lambda_{v_4}/(U_4(\Delta T_4 - \Delta T_{loss})) = (0.1658)(2358.78)/(2.0577(10.2205-2))$$
$$= 23.12 \text{ m}^2$$

$$A_5 = D_5 \lambda_{v_5}/(U_5(\Delta T_5 - \Delta T_{loss})) = (0.1639)(2385.21)/(1.9548(10.7584-2))$$
$$= 22.83 \text{ m}^2$$

$$A_6 = D_6 \lambda_{v_6}/(U_6(\Delta T_6 - \Delta T_{loss})) = (0.1621)(2412.46)/(1.8571(11.3247-2))$$
$$= 22.58 \text{ m}^2$$

The maximum difference in effect areas is equal to 0.35 m^2. Assuming an error criterion of less than 0.0001 m^2 is required, therefore, a new iteration sequence has to be initiated. The second iteration starts with calculations of the new heat transfer area

$$A_m = \frac{\sum_{i=1}^{n} A_i}{n}$$

$$= \frac{18.56 + 23.74 + 23.42 + 23.12 + 22.84 + 22.58}{6}$$

$$= \frac{134.26}{6} = 22.38 \text{ m}^2$$

A new profile for the temperature drop across the effects is then calculated

$\Delta T_1 = \Delta T_1 (A_1/A_m) = (8.7628)(18.59)/(22.38) = 7.28$ °C

$\Delta T_2 = \Delta T_2 (A_2/A_m) = (9.224)\ (23.74)/(\ 22.38) = 9.78$ °C

$\Delta T_3 = \Delta T_3 (A_3/A_m) = (9.7095)\ (23.41)/(\ 22.38) = 10.16$ °C

$\Delta T_4 = \Delta T_4 (A_4/A_m) = (10.2205)\ (23.12)/(\ 22.38) = 10.56$ °C

$\Delta T_5 = \Delta T_5 (A_5/A_m) = (10.7584)\ (22.84)/(\ 22.38) = 10.98$ °C

$\Delta T_6 = \Delta T_6 (A_6/A_m) = (11.3247)\ (22.58)/(\ 22.38) = 11.43$ °C

A new iteration is then taken, which starts with temperature profiles and continues to the convergence criteria part. Since, the specified tolerance is small, a total of 8 iterations are executed. The error criterion after the last iteration is 5.7×10^{-5} m^2, i.e., the difference between the maximum and minimum areas is equal to this value. Summary of flow rates, concentrations, temperatures, and heat transfer areas in the last iteration are given in the following table

Effect	1	2	3	4	5	6
D (kg/s)	0.1708	0.1693	0.1677	0.1662	0.1646	0.1614
B (kg/s)	2.3292	2.16	1.9922	1.826	1.6614	1.5
X (ppm)	45078.9	48611.5	52704.4	57501.2	63198.6	70000
T (°C)	92.67	84.96	76.84	68.29	59.29	40
A (m^2)	22.1446	22.1445	22.1445	22.1446	22.1446	22.1446

Finally, the system performance parameters are calculated. To obtain the performance ratio it is necessary to determine the steam flow rate, where

$M_S = D_1 \lambda_{V_1}/\lambda_S = (0.1713)(2280.7)/(2256.04) = 0.1726$ kg/s

Since the total distillate flow rate is equal to 1 kg/s, then,

$PR = M_d/M_s = 1/0.1726 = 5.79$

This is an interesting result and is consistent with MEE practice, where the performance ratio is *approximately* equal to the total number of effects.

The condenser thermal load is calculated from

$Q_c = D_6 \lambda_{v6} = (0.1614)\ (2412.46) = 389.44$ kJ/s

The logarithmic mean temperature difference in the condenser is given by

$$(LMTD)_c = (T_f - T_{cw})/Ln((T_6 - \Delta T_{loss} - T_{cw})/(T_6 - \Delta T_{loss} - T_f))$$
$$= (35\text{-}25)/Ln((40\text{-}2\text{-}25)/(40\text{-}2\text{-}35))$$
$$= 6.819\ ^oC$$

The condenser heat transfer area in the condenser is then calculated from

$A_c = Q_c/(U_c\ (LMTD)_c) = 389.44/((1.75)(6.819)) = 32.628\ m^2$

The specific heat transfer area is calculated by the summing the heat transfer areas for the six evaporators and the condenser. This is

$$sA = \frac{\sum_{i=1}^{n} A_i + A_c}{M_d} = (132.86+32.628) = 165.49\ m^2$$

The cooling water flow rate is obtained from Eq. 39

$D_6 \lambda_{v6} = (M_f + M_{cw})\ Cp\ (T_f - T_{cw})$

$(0.1614)(2412.45) = (2.5+Mcw)\ (4.2)(35\text{-}25)$

which gives $M_{cw} = 13.73$ kg/s. The specific cooling water flow rate has the same value, since the total product flow rate is equal to 1 kg/s.

Detailed Mathematical Model of MEE

The steady-state MEE model includes a set of material and energy balances, heat transfer equations, and thermodynamic relations. The main features of the model include the following:

- It maintains constant heat transfer areas in the evaporators and the feed heaters. This is common industrial practice, which is necessary to reduce the cost of construction, spare parts stocking, and maintenance.
- It considers the effect of the vapor leak to the venting system.
- It takes into consideration variations in the thermodynamic losses within the system. This includes the boiling point elevation, the non-equilibrium allowance inside the evaporators and the flashing boxes, temperature depression corresponding to the pressure drop in the demister, vapor transmission lines, and during the condensation process.
- It includes the effect of boiling temperature, brine velocity inside the tubes of feed heaters, the tube material, and the tube bundle geometry on the required heat transfer area.
- It takes into consideration temperature and salinity effects on the water physical properties such as latent heat, heat capacity, density, thermal conductivity, and viscosity.
- It weights the effect of non-condensable gases on the heat transfer coefficient in the evaporators and the feed heaters.

Assumptions used in the model include:

- The vapor formed in the effects is salt free.
- Energy losses from the effects to the surroundings are negligible. This is because of operation at relatively low temperatures, between 100-40 ^{o}C, and the effects are well insulated.
- The heat transfer efficiency in the exchange units, which include evaporators, condensers, and preheaters, is assumed constant.
- The physical properties of various streams are calculated at the temperature average of influent and effluent streams.

The mathematical model is divided into three parts, which include material balances, energy balances, and the heat transfer rate equations. Also, the model includes equations for the heat transfer coefficient, thermodynamic losses, and the physical properties. Details for these equations are given in the appendices. The following section gives the equations used to determine flow rates of various streams, temperature profiles in the effects, preheaters, and flash boxes, and the heat transfer areas in the effects, preheaters, and the down condenser.

Material Balances

The overall material and salt balances are given by

$$M_f = M_d + M_b \tag{40}$$

$$M_b = M_f (X_f / X_b) \tag{41}$$

where M is the mass flow rate, X is the salt concentration, and the subscript b, d, and f denotes the brine, the distillate, and the feed seawater. The total distillate flow rate, M_d, is defined by

$$M_d = \sum_{k=1}^{n} D_k + \sum_{k=2}^{n} d_k \qquad 42)$$

where D and d are the amounts of vapor formed by boiling and flashing, respectively, and the subscripts k and n define the effect number and the total number of effects. The difference of the total seawater feed, M_f, and the amount of vapor formed in the first effect, D_1, gives the brine flow rate leaving the first effect

$$B_1 = M_f - D_1 \qquad (43)$$

For effects 2 to n, the brine flow rate leaving effect j is given

$$B_j = M_f - \sum_{k=1}^{j} D_k - \sum_{k=2}^{j} d_k \qquad (44)$$

In Eqs. 43 and 44 B is the brine flow rate. The salt balance in the brine stream leaving the first effect and effects 2 to n is

$$X_1 = \frac{M_f X_f}{M_f - D_1} \qquad (45)$$

$$X_j = \frac{M_f X_f}{M_f - \sum_{k=1}^{j} D_k - \sum_{k=2}^{j} d_k} \qquad (46)$$

Energy balances

In the first effect, the latent heat of the condensing steam is used to increase the temperature of feed seawater from t_2 to the boiling temperature T_1 and to provide the heat required to evaporate a controlled mass of vapor, D_1 at T_1. This gives

$$M_S \lambda_S = M_f C_p (T_1 - t_2) + D_1 \lambda_{V1} \qquad (47)$$

where Cp is the specific heat at constant pressure, λ is the latent heat, T is the effect temperature, t is the seawater temperature, and the subscripts 1, 2, v and s denotes the first effect, the preheater associated with the second effect, the vapor, and the heating steam. Correlations for the specific heat at constant pressure and the latent heat are given in Appendix A. In all effects, the boiling temperature, T_j, is higher than the vapor saturation temperature, T_{vj}, by the boiling point elevation, $(BPE)_j$, and the temperature rise caused by the hydrostatic pressure head, ΔT_{yj}. This is

$$T_j = T_{vj} + (BPE)_j + \Delta T_{yj} \tag{48}$$

The term, ΔT_{yj}, is negligible in horizontal falling films, because of the very small thickness of the boiling film.

The latent heat of the vapors formed by boiling in effect j-1 is used to boil off a smaller amount of vapor in the next effect, j. The decrease in the vapor amount is caused by the increase in the vapor latent heat upon the decrease in effect temperature, i.e., $T_{cj-1} > T_{vj}$ and $\lambda_{cj-1} < \lambda_{vj}$. This energy balance is

$$D_j = \frac{D_{j-1}\lambda_{cj-1}}{\lambda_{vj}} \tag{49}$$

In Eq. 49 the boiling process occurs on the outer surface of the evaporator tubes. The condensation temperature, T_{cj}, is lower than the effect temperature, T_j, by the boiling point elevation, $(BPE)_j$, and the saturation temperature depressions associated with pressure losses in the demister, $(\Delta P_p)_j$, transmission lines between the effects, $(\Delta P_t)_j$, and vapor condensation inside the tubes, $(\Delta P_c)_j$. The resulting condensation temperature is

$$T_{cj} = T_j - (BPE + \Delta T_p + \Delta T_t + \Delta T_c)_j \tag{50}$$

The pressure drop during condensation, ΔP_c, is defined as the algebraic sum of the decrease caused by friction, ΔP_r, and the increase caused by gravity (ΔP_g) and vapor deceleration (ΔP_a). This relation is given by

$$\Delta P_{cj} = (\Delta P_r - \Delta P_g - \Delta P_a)_j \tag{51}$$

Correlations for the pressure drop components, ΔP_p, ΔP_t, ΔP_r, ΔP_g, and ΔP_a are given in Appendix B.

As the brine enters the second effect, which is at a lower pressure, it flashes and consequently its temperature is reduced from T_1 to T'_2. The flashing process forms a small amount of vapor, d_2, which is used to preheat partially the feed seawater in the effect preheater. Similar, processes take place in effects 3 to n. The energy balance for this process in the second effect and effects 3 to n is given by

$$d_2 = (M_f - D_1)\, C_p \frac{T_1 - T'_2}{\lambda'_{v_2}} \tag{52}$$

$$d_j = \left(M_f - \sum_{k=1}^{j} D_k - \sum_{k=2}^{j} d_k \right) C_p \frac{T_{j-1} - T'_j}{\lambda'_{v_j}} \tag{53}$$

where λ'_{v_j} is the latent heat of formed vapor at T'_j. In Eq. 53, the brine flowing into effects 3 to n is reduced by the amounts of boiled and flashed off vapors. In effects 2 to n, the boiling temperature within the effect, T_j, is lower than the temperature of flashing brine, T'_j, by the non-equilibrium allowance $(NEA')_j$;

$$T'_j = T_j + (NEA')_j \tag{54}$$

The correlation for the non-equilibrium allowance is given in Appendix B.

The formed vapor in the first effect, D_1, condenses as it releases its latent heat in the second effect. This condensate enters the flashing box associated with second effect. The flashing process reduces the temperature of condensed vapor from T_{c_1} to T''_2. The value of T''_2 is higher than the vaporization temperature within the flash box, T''_{v_2}, by the non-equilibrium allowance for the flash box $(NEA'')_2$. The same process takes place in the flashing boxes of effects 3 to n and the resulting relation between T''_{v_j} and T''_j is given by

$$T''_j = T''_{v_j} + (NEA'')_j \tag{55}$$

The energy balance in flash boxes in the second effect and effects 3 to n gives the flow rate of amount of formed vapor.

$$\bar{d}_2 = D_1 C_p \frac{(T_{c_1} - T''_2)}{\lambda''_{v_2}} \tag{56}$$

$$\bar{d}_j = \left(\sum_{k=1}^{j} D_k + \sum_{k=2}^{j-2} d_k \right) C_p \frac{\left(T_{c_{j-1}} - T_j'' \right)}{\lambda_{v_j}''} \tag{57}$$

where λ''_{v_j} is the latent heat of vaporization at T''_{v_j}. As shown in Eqs. 56 and 57, the amount of condensing vapor entering the flash box in the second effect is equal to D_1. This amount increases in subsequent flash boxes by the amount of vapor formed by boiling and flashing within these effects.

At the other end of the flow diagram, in the down condenser, the temperature of the intake seawater, $M_{cw}+M_f$, is increased from T_{cw} to T_f. The heating energy is provided by condensation of the vapors formed by flashing and boiling in the last effect and by flashing in the associated flash box. This is given by

$$\eta_n \left(d_n \lambda'_{c_n} + \bar{d}_n \lambda''_{c_n} + D_n \lambda_{c_n} \right) = \left(M_{cw} + M_f \right) C_p \left(T_f - T_{cw} \right) \tag{58}$$

where η is the heat exchange efficiency and the subscripts c, cw, and n denote the condensing vapors, the intake seawater, and the last effect. The energy source in the feed preheaters in effects 2 to n-1 is the latent heat of condensation for the vapors formed by flashing inside the effect and the flash boxes. This balance is

$$\eta_j \left(d_j \lambda'_{c_j} + \bar{d}_j \lambda''_{c_j} \right) = M_f C_p (t_j - t_{j+1}) \tag{59}$$

In Eqs. 58 and 59 λ''_{c_j} and λ''_{c_j} are the latent heat of condensation of flashed vapors in the feed preheaters at T'_{c_j} and T''_{c_j}. These temperature are lower than the vapor temperatures, T'_{v_j} and T''_{v_j} by the depression in the saturation temperature caused by pressure loss in the demister and during condensation outside the preheater tubes. These relations are

$$T'_{c_j} = T'_{v_j} - \Delta T'_{p_j} - \Delta T'_{c_j} \tag{60}$$

$$T''_{c_j} = T''_{v_j} - \Delta T''_{p_j} - \Delta T''_{c_j} \tag{61}$$

The correlation for the pressure loss in the demister is given in Appendix B. As for the condensation pressure loss it is assumed negligible, since the friction losses are compensated by the hydrostatic deceleration gains, Muller, 1991.

Heat Transfer Design Equations

The design equations for the heat transfer area are developed for the evaporators, the preheaters, and the down condenser. For the evaporators, the heat transfer area, A_e, is

$$A_e = \frac{M_s \lambda_s}{U_{e1}(T_s - T_1)} = \frac{D_j \lambda_{v_j}}{U_{ej}(T_{c_{j-1}} - T_j)} \tag{62}$$

where U is the overall heat transfer coefficient, the subscript j defines effects 2 to n, and the subscript e refers to the evaporator. As discussed before and as shown in Eq. 47, the thermal load in the first effect differs from other effects by the energy consumed to increase the seawater temperature from t_2 to T_1. In other effects, the feed brine is at the saturation temperature and the effect thermal load is equivalent to the vaporization latent heat.

The following relation gives the heat transfer area in the preheaters of effects 2 to n-1

$$A_{hj} = \frac{M_f C_p (t_j - t_{j+1})}{U_{h_j}(LMTD)_j} \tag{63}$$

$$(LMTD)_j = \frac{t_j - t_{j+1}}{\ln \dfrac{T'_{cj} - t_{j+1}}{T'_{c_j} - t_j}} \tag{64}$$

Similarly, the heat transfer area of the down condenser is given by

$$A_c = \frac{(M_f + M_{cw}) C_p (T_f - T_{cw})}{U_c A_c (LMTD)_c} \tag{65}$$

$$(LMTD)_c = \frac{T_f - T_{cw}}{\ln \dfrac{T'_{cn} - T_{cw}}{T'_{cn} - T_f}} \tag{66}$$

The overall heat transfer coefficient in Eqs. 62, 63, and 65 is based on the outside surface area and is related to the individual thermal resistance by the following expression.

$$\frac{1}{U_o} = \frac{1}{h_i}\frac{r_o}{r_i} + R_{f_i}\frac{r_o}{r_i} + \frac{r_o \ln(r_o/r_i)}{k_w} + R_{f_o} + \frac{1}{h_o} \tag{67}$$

where h is the heat transfer coefficient, R_f is the fouling resistance, k_w is the thermal conductivity of tube material, and r is the tube radius. The subscript i and o refer to the inner and outer tube surface, respectively. Correlations for the individual heat transfer coefficient are given in Appendix C.

Solution Method of the Detailed MEE Model

The developed model contains a large number of highly non-linear algebraic equations. The equations are solved by a modified fixed point iteration technique developed by El-Dessouky and Bingulac, 1996. The method is simple, but yet powerful and has proved to have a rapid convergence rate. The solution process starts with setting values of system parameters, which include salinity of intake seawater and rejected brine, temperature of intake seawater, temperature of rejected cooling seawater, and boiling temperature in effect n, tube length and diameter, vapor and brine velocities inside the tubes, evaporator area (constant in all effects), and area of preheaters in effects 2 to n-1. Initial guess is made for the temperature profiles in the effects and the preheaters. Iterations are performed in two loops on the preheaters and the evaporators. Solution starts at the last effect and proceeds towards the first effect. Completion of the iterative procedure results in determination of the temperature profiles, salt concentration profile, and flow rates of brine and distillate. Results are used to determine other system parameters, which include the performance ratio, the specific heat transfer area, and the specific cooling seawater flow rate.

The system parameters used in generating the model results are:

- The seawater temperature, T_{cw}, and salinity, X_f, are 25°C and 42000 ppm.
- The salinity of rejected brine, X_b, is 70000 ppm
- The temperature of rejected cooling water, T_f, is 35°C.
- The boiling temperature in the last effect, T_n, is 40°C.
- The sum of the fouling heat transfer resistance inside and outside the tubes in the preheaters and the evaporators, $R_{f_i}+R_{f_o}$, is $1.75\text{x}10^{-4}$ m^2 °C/W.
- The thermal efficiency of the preheaters, η_i, is 90%.
- The tube outside and inside diameters, δ_o and δ_i, are 31.75 mm 19.75 mm.
- The brine velocity, V, inside the preheater tubes is 1.55 m/s.
- The range for the top brine temperature in the first effect is 60-110 °C.
- The range for the number of effects is 4-12.

4.2.3 System Performance

The developed model for MEE system is validated through analysis of the effect and preheater characteristics. This includes analysis of profiles for the temperature and the distillate flow rates across the effects. Further analysis includes variations in the system performance parameters as a function of the number of effects and the top brine temperature.

The temperature profiles in the effects and the preheaters are shown in Fig. 5. The nonlinear form of both profiles across the effects and the preheaters indicates higher temperature drop per effect close to the cold side of the effects, i.e., effect number n. Since the heat transfer area is constant in all effects and preheaters and the overall heat transfer coefficients are larger at higher temperatures, it is necessary to have larger temperature drop at the cold side of the effects in order to compensate the reduction in the coefficient value. Similar thermal loads in the effects and the preheaters dictate this behavior. This is shown in the relation given by Eq. 49, where the rate of the latent heat of condensation of formed vapor in effect j is equivalent to the rate of the latent heat of evaporation of formed vapor in effect j+1.

Figure 6 include profiles for the distillate flow rates generated in the flash box and in the effect by boiling and flashing. Results indicate that the major portion of the total product is formed by evaporation within the effect. In addition, evaporation rates are higher at the first effect and decreases in subsequent effects. The relation given by Eq. 49, where the latent heat of vaporization is smaller at higher temperatures, dictates this behavior. Figure 6, show that the amount of distillate formed by flashing inside each effect is negligible in comparison with that formed in the flash boxes. In each effect, the flow rate of flashing vapors is close to 10% of the amount formed by boiling. Irrespective of this, the small amount of flashing vapors posses sufficient heat to increase the temperature of the feed seawater from a low value of 25 ^{o}C to higher temperatures close to the top brine temperature.

Figure 7 illustrates the effect of the top brine temperature and the total number of effects on the performance ratio of the system. As is shown, the performance ratio is nearly independent of the top brine temperature and is strongly related to the number of effects. This behavior is explained in terms of the distillate flow rate profiles shown in Fig. 6 for a 12 effect system. As is shown, the amount of distillate formed at high temperature side is close to 1 kg/s. This rate decreases at the low temperature side of the effects to values close to 0.7 kg/s. Irrespective of this, the amount of distillate formed at the low temperature side a sizeable fraction of the total product flow rate. Therefore, increase of the

number of effects allows for increase in the number of steam reuse and the formation of additional amounts of distillate.

Variations in the specific heat transfer area as a function of the top brine temperature and the number effects are shown in Fig. 8. As is shown, the required heat transfer area per unit mass of product water increases by using a larger number of effects and reducing the top brine temperature. The use of a larger number of effects decreases the temperature drop per effect or the driving force for heat transfer. Therefore, keeping the top brine temperature constant and increasing the number of effects results in the increase of the specific heat transfer area. On the other hand, keeping the number of effects constant and increasing the top brine temperature result in the increase of the overall heat transfer coefficient. This reduces the thermal resistance and gives smaller heat transfer areas. At the highest top brine, the specific heat transfer area is almost independent on the number of effects. As is show in Fig. 8, all profiles converges to lower value at the highest top brine temperature. This is caused by the increase in the temperature drop per effect, especially at a larger number of effects.

Effects of the top brine temperature and the number of effects on the specific cooling water flow rate are shown in Fig. 9. Variations in the specific cooling water flow rate of cooling are insensitive to the value of the top brine temperature. On the other hand, the specific cooling water flow rate decreases rapidly upon the increase of the number of effects. As previously shown in Fig. 8 the system performance ratio is independent on the top brine temperature, where the amounts of distillate generated and steam used vary slightly as the top brine temperature increases. As a result, the amount of vapor formed in the last effect, which is condensed by the cooling seawater, varies slightly as the top brine is increased. This results in negligible variations in the specific cooling water flow rate as the top brine temperature is increased. Increasing the number of effects increases the total amount of product fresh water and reduces the amount of distillate formed per effect. In turn, a smaller amount of cooling seawater is needed to operate the condenser. The net result is a rapid decline in the specific cooling water flow rate.

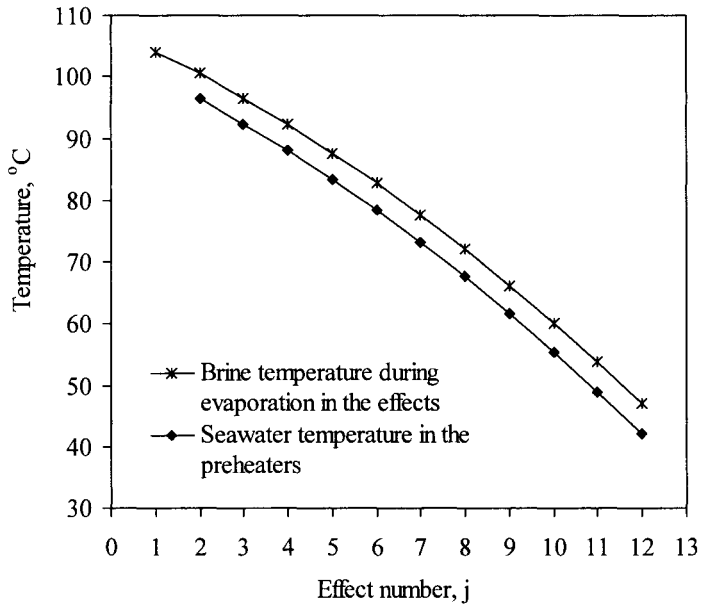

Fig. 5. Variation in temperature profiles in the evaporator and the preheater.

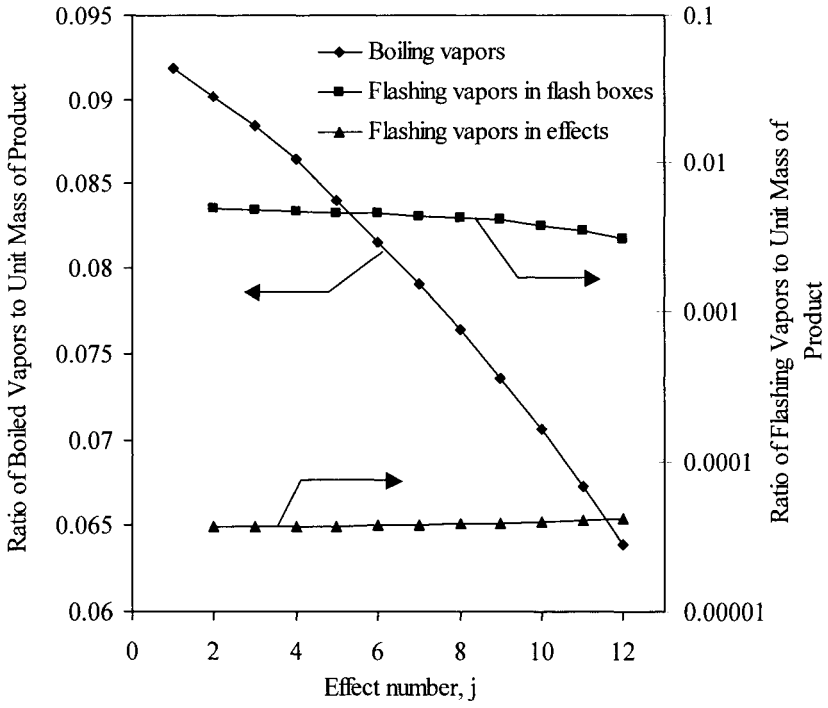

Fig. 6. Variation in distillate profiles as a function of effect number at $T_s = 100\ ^oC$.

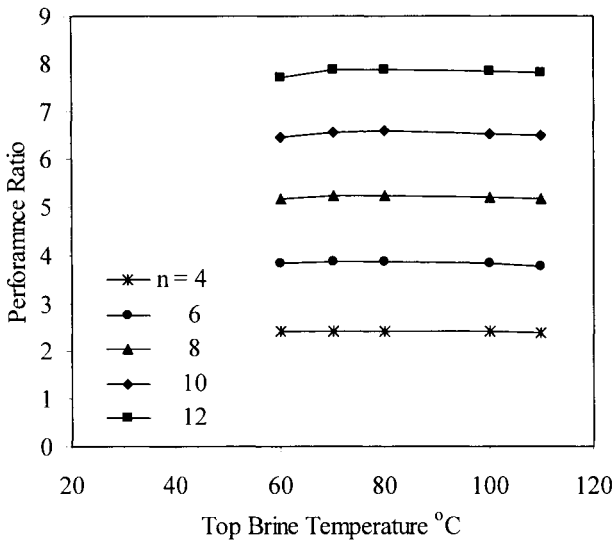

Fig. 7. Variation in the performance ratio as a function of top brine temperature and the number of effects.

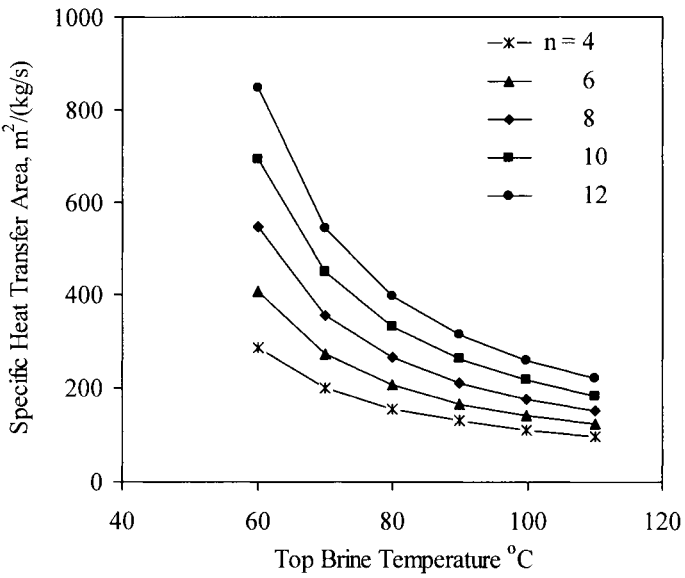

Fig. 8. Effect of top brine temperature and the number of effects on the specific heat transfer area.

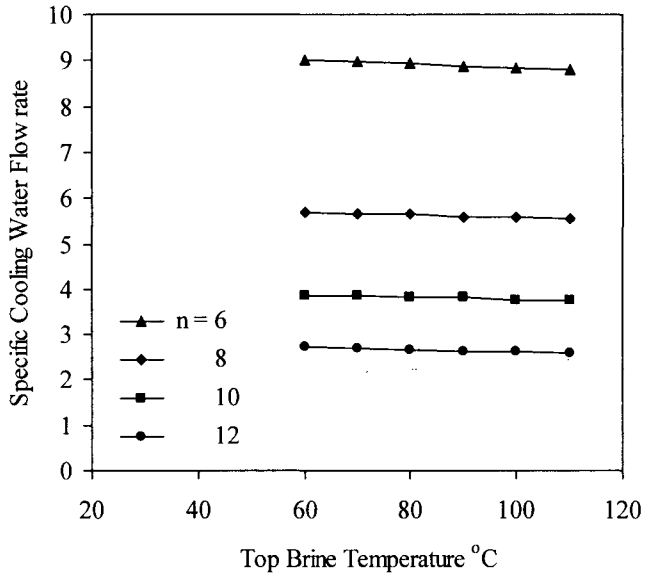

Fig. 9. Effect of top brine temperature and the number of effects on the specific cooling water flow rate.

4.2.4 Summary

The following conclusions are made in the light of the results and discussion given in the previous section:

- Modeling of the MEE system must take into consideration the nonlinear behavior of the governing equations. This is necessary to obtain complete descriptive model suitable for design, simulation, and analysis of existing and new systems. Simplified models with linear profiles have limited value and caution should be made in use of its predictions.
- Vapor formation by boiling and flashing is essential in modeling the effects, flash boxes and preheaters.
- The performance ratio of the MEE system is virtually independent of the top brine temperature and is strongly affected by the number of effects. A larger number of effects increase the number of vapor reuse and consequently the total amount of vapor formed.
- Operation of the MEE system at higher top brine temperature results in drastic decrease in the specific heat transfer area. This is because of the increase in the temperature driving force per effect and the heat transfer coefficient.

- The specific cooling water flow rate is independent of the top brine temperature. This is because the temperatures of the vapor in the last effect and the seawater leaving the down condenser are kept constant.
- The specific cooling water flow rate is reduced rapidly as the number of effects is increased, this is because of the reduction in the amount of vapor formed per effect, which reduces the thermal load in the down condenser.
- Comparison of values for the overall heat transfer coefficient predicted by the developed model show consistent behavior with literature data. The coefficient data with fouling are lower than literature data with clean surfaces. However, removal of the fouling effect gives values similar to literature correlations.

References

El-Dessouky, H.T., and Bingulac, S., Solving equations simulating the steady-state behavior of the multi-stage flash desalination process, Desalination, **107**(1996)171-193.

El-Dessouky, H.T., Alatiqi, I., Bingulac, S., and Ettouney, H.M., Steady-state analysis of the multiple effect evaporation desalination process, Chem. Eng. Tech., **21**(1998)437-451.

Muller, A.C., Condensers, Handbook of Heat Exchanger Design, Hewitt, G.F., Editor, Hemisphere, N.Y., 1991.

Rautenbach, R., and Schafer, S., Calculation of stagewise fouling factors from process data of large MSF distillers, Proceeding of the IDA World Congress on Desalination and Water Sciences, Madrid, Spain, October, 1997, Vol. I, pp 165-177.

Temstet, C., Laborie, J., and et al., Dual purpose desalination plant-high efficiency multiple-effect evaporator operating with a turbine for power production, Proceedings of the IDA World Congress on Desalination and Water Sciences, Abu Dhabi, November, 1995, Vol. III, 297-308.

Temstet, C., Canton, G., Laborie, J., and Durante, A., A large high-performance MED plant in Sicily, Desalination, **105**(1996)109-114.

Problems

1. A four effect MEE system operates at the following conditions:
   - Intake seawater temperature = 25 °C.
   - Intake seawater salinity = 35,000 ppm.
   - Rejected brine temperature = 35 °C.

- Top brine temperature = 95 °C.
- Flow rate of distillate product = 50 kg/s
- Heat transfer area of brine heater of the third effect = 80.7 m2.
- Heat transfer area of each effect = 723.3 m^2.
- Heat transfer coefficient in effect 1 = 5.2 kW/m^2 °C.
- Heat transfer coefficient in effect 2 = 3 kW/m^2 °C.
- Heat transfer coefficient in effect 3 = 2.1 kW/m^2 °C.
- Temperature of cooling water = 30 °C.
- Temperature of brine flow from third effect preheater = 50 °C.
- Boiling point elevation in each effect = 1 °C.
- The mass of vapor formed in each stage is constant.

Calculate the plant performance ratio, the specific heat transfer area, the mass flow rate of cooling water, and mass of vapor formed by flashing in the flashing box of the third effect.

2. A five effect MEE system operates at the following conditions:
   - Intake seawater temperature = 40 °C.
   - Intake seawater salinity = 42,000 ppm.
   - Heating steam temperature = 112 °C.
   - Temperature of vapor in last effect = 55 °C.
   - Thermodynamic losses other than BPE = 0.45 °C
   - Specific heat at constant pressure of seawater = 4.1 kJ/kg °C.
   - Flow rate of distillate product = 2000 kg/s
   - Temperature of cooling water = 45 °C.
   - Heat transfer coefficient in effect 1 = 5.25 kW/m^2 °C.
   - Heat transfer coefficient in effect 2 = 5.1 kW/m^2 °C.
   - Heat transfer coefficient in effect 3 = 4.85 kW/m^2 °C.
   - Heat transfer coefficient in effect 4 = 4.3 kW/m^2 °C.
   - Heat transfer coefficient in effect 5 = 3.7 kW/m^2 °C.

Calculate the plant performance ratio, the specific heat transfer area, the mass flow rate of cooling water, and mass of vapor formed by flashing in the flashing box of the third effect.

3. A three effect MEE system operates at the following conditions:
   - Plant capacity = 500 ton/day.
   - Steam temperature = 110 °C.
   - Intake seawater salinity = 42,000 ppm.
   - Temperature of vapor in last effect = 40 °C.
   - Intake seawater temperature = 20 °C.
   - Heat transfer coefficient in effect 1 = 3.123 kW/m^2 °C.
   - Heat transfer coefficient in effect 2 = 1.987 kW/m^2 °C.
   - Heat transfer coefficient in effect 3 = 1.136 kW/m^2 °C.

Calculate the plant performance ratio, the specific heat transfer area, and the mass flow rate of cooling water.

4. A three effect MEE system operates at the following conditions:
   - Plant capacity = 5 kg/s.
   - Steam temperature = 115 °C.
   - Intake seawater salinity = 42,000 ppm.
   - Specific heat at constant pressure of seawater = 4.18 kJ/kg °C.
   - Load of the third effect = 13.5 kN/m^2.
   - Intake seawater temperature = 27 °C.
   - Heat transfer coefficient in effect 1 = 4 kW/m^2 °C.
   - Heat transfer coefficient in effect 2 = 3 kW/m^2 °C.
   - Heat transfer coefficient in effect 3 = 2.5 kW/m^2 °C.

Calculate the plant performance ratio, the specific heat transfer area, and the mass flow rate of cooling water.

4.3 *Parallel Feed Multiple Effect Evaporation*

A large number of the parallel feed multiple effect evaporation is found in the desalination industry and it accounts for 3% of the total desalination market, IDA (2000). The process is found in the stand-alone mode or combined with thermal or mechanical vapor compression. The process has evolved from small production units with capacities less than 5000 m^3/d to larger units with capacities close to 20000 m^3/d, which are competitive to the MSF process.

Figures 2a and 2b show the operating lines for two possible configurations for the process as a function of the stream salinity and temperature. In both diagrams the horizontal line represent the feed stream to each effect. As is shown for all effects the feed has the same temperature and salinity. Inside the effect the feed temperature is increased to saturation conditions. This followed by evaporation and increase in salinity, which is represented by the vertical lines. Further discussion and details for this diagram are given in the following sections.

4.3.1 *Process Description*

Process schematics for the parallel-feed multiple-effect evaporation are shown in Figs. 10 and 11. The effects are numbered 1 to n from the left to right (the direction of the heat flow). Each effect constitutes a heat transfer area, vapor space, mist eliminator and other accessories. In the parallel feed system, the vapor flows from left to right, in the direction of falling pressure, while the feed seawater flows in a perpendicular direction. As for the parallel/cross flow system, Fig. 11, the brine stream leaving the first stage flows to the second, where it flashes and mixes with the feed seawater. Either system contains a number of evaporators, a train of flashing boxes, a down condenser, and a venting system. The parallel and the parallel/cross flow systems contain (n-1) flashing boxes for the distillate product. In the parallel/cross flow system, brine flashing takes place inside effects 2 to n. The two configurations utilize the horizontal falling film tubes, which are characterized by their ability to handle seawater scaling. This is because of the high wetting rates and efficient water distribution over the heat transfer surfaces by large spray nozzles. Thus, dry-patch formation or water mal-distribution is eliminated. This configuration offers the additional advantages of positive venting and disengagement of vapor products and/or non-condensable gases, high heat transfer coefficients, and monitoring of scaling or fouling materials.

The intake seawater is introduced into the down condenser, where it absorbs the latent heat of the condensing vapor from the last effect. As a result, intake seawater temperature increases to the feed temperature. Part of the

heated intake seawater is rejected back to the sea, which is known as the cooling seawater. The function of cooling seawater is the removal of the excess heat added to the system in the first effect. The feed seawater stream is chemically treated, deaerated, and sprayed into the effects. The seawater spray falls in the form of thin film down the succeeding rows of tubes arranged horizontally. Within each effect, the brine temperature is increased to the boiling temperature corresponding to the pressure in the vapor space before a small portion of water vapor is formed. In the first effect, the heat required for preheating and evaporation is provided by condensing a controlled mass of saturated steam inside the tube bundle. The steam is supplied to the system from an external boiler. The high quality condensate from the first effect is returned back to the boiler.

The saturation temperature of the vapor formed in each effect is less than the brine boiling temperature inside the effect by the boiling point elevation. The vapor generated in each effect flows through a knitted wire mist separator known as wire mesh demister to remove the entrained brine droplets. The saturation temperature of the vapor departing the demister is less than that of the formed vapor due to the frictional pressure loss in the demister. The vapor flows from the demister has to be transported to the second effect. This transport inevitably involves a pressure drop and hence a corresponding decrease in the saturation temperature. Another pressure fall and consequent depression in the saturation temperature of the vapor is associated with vapor condensation inside the heat transfer tubes in the evaporators or over the heat transfer area in the preheaters. The latent heat of condensation of the vapor is exploited for further evaporation in the second effect.

In the parallel/cross system, the vapor formed in effects 2 to n is by boiling over the heat transfer surfaces and by flashing or free boiling within the liquid bulk. The temperature of the vapor formed by flashing is less than the effect boiling temperature by the boiling point elevation and the non-equilibrium allowance. Another small quantity of vapor is formed in the flashing box due to the flashing of distillate condensed in effect i. The flashed off vapor is produced at a temperature lower than the distillate condensation temperature by the non-equilibrium allowance. The flashing boxes offer a means for recovering heat from condensed fresh water and the brine stream. The boiling point elevation and temperature depression corresponding to pressure loss in the demister, transmission lines and during the condensation process reduces the available driving force for heat transfer in the evaporators and the preheaters. Thus, it is necessary to provide excess surface areas to compensate for these temperature degradations. In other words, the temperature losses present an extra resistance to the flow of heat between the condensing steam and the boiling seawater. Nonetheless, the temperature downgrading does not influence the plant thermal performance ratio or steam economy. The plant performance ratio depends on heat balance consideration and not on the rate of heat transfer. In the

parallel/cross flow system the vapor formed by brine flashing from stage i are condensed inside the tube side of effect i+1. However, all vapors from the last effect are condensed on the shell side in the down condenser.

The amount of steam generated by evaporation in each effect is less than the amount generated in the previous effect. This is due to increase in the specific latent heat of vaporization with the decrease in the effect temperature. Consequently, the amount of vapor generated in an evaporator by boiling is less than the amount of condensing steam used for heating in the following evaporator. In either configuration, the salinity of the brine stream leaving each effect is close to solubility limit of $CaSO_4$, Figs. 2a. The brine stream leaving the last effect in the parallel or the parallel/cross systems is rejected back to the sea.

The down condenser is provided by good vents, first for purging during start-up and then for removing non-condensable gases, which may have been introduced with the feed or due to inleakage. The presence of the non-condensable gases not only impedes the heat transfer process but also reduces the temperature at which steam condenses at the given pressure. This occurs partially because of the reduced partial pressure of vapor in a film of poorly conducting gas at the interface. To help conserve steam economy venting is usually cascaded from the steam chest of one evaporator to another. The effects operate above atmospheric pressure are usually vented to the atmosphere. The non-condensable gases are always saturated with vapor. The vent for the bottom condenser must be connected to vacuum-producing equipment to compress the non-condensable gases to the atmosphere. This is usually a steam jet ejector if high-pressure steam is available. Steam jet ejectors are relatively inexpensive but also quite inefficient. Since the vacuum is maintained on the last effect, the unevaporated brine flows by itself from effect to effect and only a blow down pump is required in the last effect.

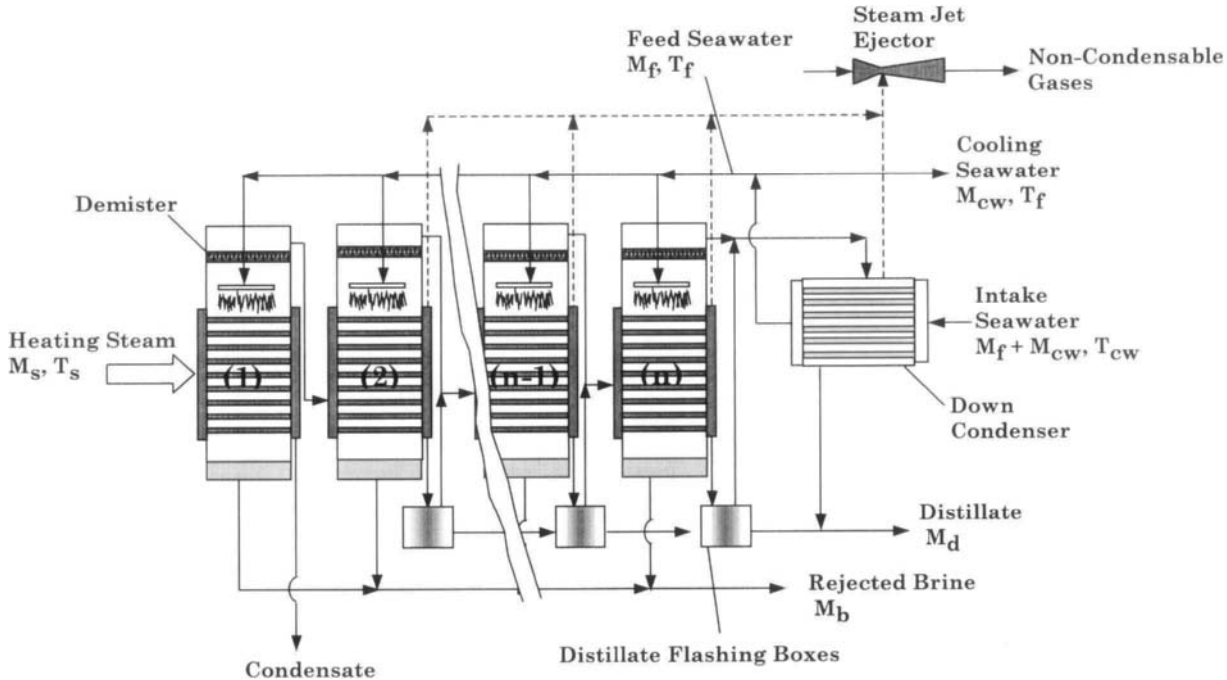

Fig. 10. Schematic of MEE parallel flow

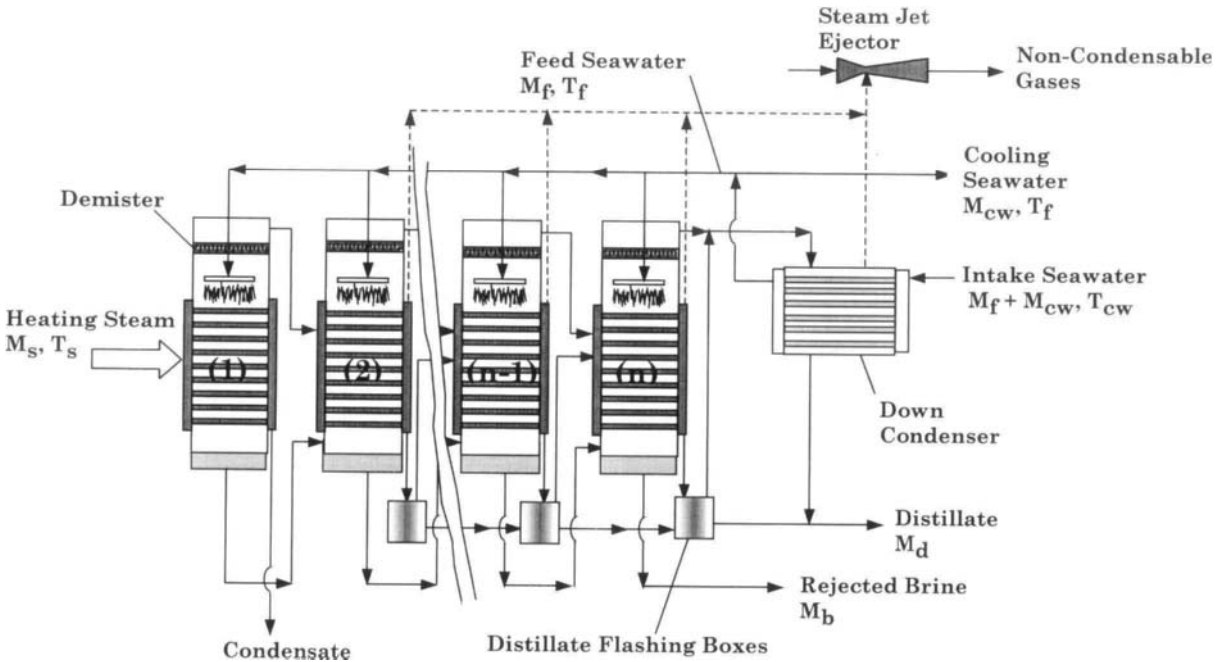

Fig. 11. Schematic of MEE parallel/cross flow

4.3.2 Process Modeling

The mathematical models of the parallel and parallel/cross flow MEE systems include basic material and energy balance equations as well as correlations for estimating the heat transfer coefficients, the thermodynamic losses, pressure drops, and physical properties. Results are reported in terms of the thermal performance ratio, the specific heat transfer area, the specific cooling water flow rate, and the conversion ratio. Other data include profiles of the effect temperature, pressure, flow rate, and salinity. The following two sections include model equations for the parallel and parallel/cross systems. Two assumptions are used in the analysis; the first assumes the system to be at steady state conditions and the second assumes that the distillate is salt free. The second assumption implies negligible entrainment of the brine droplets by the formed vapor.

Features of the developed mathematical models include the following:

- Constant and equal heat transfer areas in all effects, which is the standard practice in design of thermal desalination system.
- The heat transfer equations model the heat transfer area in each evaporator as the sum of the area for brine heating and the area for evaporation.
- Model variations in the thermodynamic losses (boiling point elevation, non-equilibrium allowance inside the evaporators and the flashing boxes, temperature depression corresponding to the pressure drop in the demister, vapor transmission lines, and during the condensation process) from one effect to another.
- Study the effect of boiling temperature, the velocity of brine flowing through the down condenser tubes, the tube material of construction, and the tube bundle geometry on the required specific heat transfer area.
- Variable physical properties of water.
- Weight the effect of the presence of non-condensable gases on the heat transfer coefficients in the evaporators and down condenser.

Mathematical Model of the MEE Parallel Flow

The mathematical model for the MEE parallel flow system includes the material and energy balance equations as well as the heat transfer equations for each effect, the flashing boxes, and the down condenser. The model includes the following equations:

- Total balance in effect i

$$F_i = D_i + B_i \tag{68}$$

- Salt balance in effect i

$$X_{F_i} F_i = X_{B_i} B_i \tag{69}$$

- Energy balance in effect i

$$D_{i-1} \lambda_{i-1} + d'_{i-1} \lambda'_{i-1} = F_i C_p (T_i - T_f) + D_i \lambda_i \tag{70}$$

In Eq. (70) the first term corresponds to the heat added to the effect by condensing the vapor generated in the previous effect. This only applies to effects 2 to n, since heating steam from an external source is used to drive the system and heat the first effect. The second term, which applies only to effects 3 to n, corresponds to the heat added to the effect by condensing the vapor generated in the distillate flashing box associated with the previous effect. The third term in Eq. 3 gives the amount of heat gained by the feed stream, where its temperature is increased inside the effect from the seawater temperature to the brine boiling temperature. The last term gives the amount of heat needed to generate the vapor inside the effect. In the above equation the specific heat at constant pressure depends on the brine salinity and temperature, while the latent heat depends on the vapor temperature. Correlations for the two properties are given in Appendix A.

- Vapor temperature in effect i

$$T_{v_i} = T_i - BPE_i \tag{71}$$

where T_v is the vapor temperature.

- The vapor condensation temperature

$$T_{c_i} = T_i - BPE_i - \Delta T_p - \Delta T_t - \Delta T_c \tag{72}$$

In Eq. 72, the condensation temperature, T_{c_i}, is lower than the brine boiling temperature, T_i, by the boiling point elevation and the losses caused by pressure depression in the demister (ΔT_p), friction in the transmission line (ΔT_t), and during condensation (ΔT_c).

- Flow rate of vapor flashed off in the distillate flashing boxes

$$d'_i = D_{i-1} C_p \frac{(T_{c_{i-1}} - T''_i)}{\lambda'_i} \tag{73}$$

with

$$T''_i = T_{v_i} + (NEA)_i \tag{74}$$

where $(NEA)_i$ is the non-equilibrium allowance and is equal to $(NEA)_i = 0.33\frac{(T_{c_{i-1}} - T_i'')}{T_{v_i}}$, T_i'' is the temperature to which the accumulated distillate stream, formed in previous effects, cools down to as it enters the flashing box, Miyatake et al. (1973).

- Evaporator heat transfer area in effect i

$$D_{i-1}\,\lambda_{i-1} + d'_{i-1}\,\lambda'_{i-1} = F_i\,C_p\,(T_i - T_f) + D_i\lambda_i = A_{1i}\,U_{1i}\,(LMTD)_i + A_{2i}\,U_{2i}\,(T_{v_i} - T_i) \quad (75)$$

$$\alpha(D_{i-1}\,\lambda_{i-1} + d'_{i-1}\,\lambda'_{i-1}) = D_i\lambda_i = A_{2i}\,U_{2i}\,(T_{v_i} - T_i) \quad (76)$$

$$(LMTD)_i = (T_i - T_f)/\ln((T_{v_i} - T_f)/(T_{v_i} - T_i)) \quad (77)$$

where A_{1i} is the heat transfer area for brine heating, A_{2i} is the heat transfer area for evaporation, U_{1i} and U_{2i} are the corresponding overall heat transfer coefficients, and α is the fraction of input heat consumed by vapor formation.

- Energy balance and heat transfer area of the down condenser

$$(d'_n + D_n)\lambda_n = (M_{cw} + M_f)\,Cp\,(T_f - T_{cw}) \quad (78)$$

$$(d'_n + D_n)\lambda_n = U_c\,A_c\,(LMTD)_c \quad (79)$$

$$(LMTD)_c = (T_f - T_{cw})/\ln((T_{v_n} - T_{cw})/(T_{v_n} - T_f)) \quad (80)$$

Mathematical Model of the MEE Parallel/Cross Flow

The mathematical model for the MEE parallel/cross flow system is developed in a similar manner to the parallel flow system and it includes the following equations:

- Total balance in effect i

$$F_i + B_{i-1} = D_i + B_i \quad (81)$$

- Salt balance in effect i

$$X_{F_i}\,F_i + X_{B_{i-1}}\,B_{i-1} = X_{B_i}\,B_i \quad (82)$$

- Energy balance for effect i

$$D_{i-1}\,\lambda_{i-1} + d_{i-1}\,\lambda_{i-1} + d'_{i-1}\,\lambda'_{i-1} = F_i\,C_p(T_i - T_f) + D_i\lambda_i \tag{83}$$

- Flow rate of vapor formed by brine flashing inside the effect

$$d_i = B_{i-1}\,Cp\,\frac{T_{i-1} - T_i'}{\lambda_i} \tag{84}$$

with

$$T_i' = T_i + NEA_i \tag{85}$$

where T_i' is the temperature to which the brine cools down to as it enters the effect. As given by Eq. 84 this temperature is lower than the effect brine temperature by the non equilibrium allowance.
Heat transfer area in effect i

$$D_{i-1}\,\lambda_{i-1} + d_{i-1}\,\lambda_{i-1} + d'_{i-1}\,\lambda'_{i-1} = F_i\,C_p(T_i - T_f) + D_i\lambda_i$$
$$= A_{1i}\,U_{1i}\,(LMTD)_i + A_{2i}\,U_{2i}\,(T_{vi} - T_i) \tag{86}$$

$$\alpha(D_{i-1}\,\lambda_{i-1} + d_{i-1}\,\lambda_{i-1} + d'_{i-1}\,\lambda'_{i-1}) = D_i\lambda_i = A_{2i}\,U_{2i}\,(T_{vi} - T_i) \tag{87}$$

Energy balance and heat transfer area of the down condenser

$$(d_n + d'_n + D_n)\lambda_n = (M_{cw} + M_f)\,Cp\,(T_f - T_{cw}) \tag{88}$$

$$(d_n + d'_n + D_n)\lambda_n = U_c\,A_c\,(LMTD)_c \tag{89}$$

It should be noted that the model equations for the flow rate of vapor flashed off in the distillate flashing boxes and the logarithmic mean temperature differences in the effects and down condenser are identical to those given in the model of the MEE parallel flow system. Also, the symbols used in Eqs. 81-89 are the same as those for Eqs. 68-80. Models for the overall heat transfer coefficients in the evaporator and the down condenser are summarized in Appendix C.

Solution Algorithm

The model equations for either system are interlinked and highly nonlinear. Therefore, iterative solution is necessary to calculate the system characteristics. The solution algorithm starts with definition of the following parameters:
Number of effects are 4, 6, 8, or 12.
The heating steam temperature varies over a range of 60-100 °C.
The intake seawater temperature (T_{cw}) is 25°C.

The feed seawater temperature (T_f) is 35°C.
The boiling temperature in the last effect (T_n) is 40°C.
The seawater salinity has values of 34,000 ppm or 42,000 ppm.
The sum of the heat transfer resistances due to the tube material, fouling inside and outside the tube is 731×10^{-6} m^2 °C/W.
The tubes outside diameter (δ_o) is 31.75 mm and inside diameter (δ_i) is 19.75 mm.

The model equations for both systems are solved simultaneously by Newton's method to calculate the following:
- Flow rates of the feed, brine, and distillate in each effect.
- The steam flow rate.
- The brine temperature in effects 1 to n-1.
- The fraction of heat consumed by evaporation in each effects.
- The heat transfer areas for vapor formation and brine heating in each effect.

The iterative procedure is based on Newton's method with an iteration error of 1×10^{-4}. To facilitate the conversion procedure, each equation is scaled by the largest term found in the equation. Therefore, all equations are in the order of one. For example, the salt balance equation is rearranged into the following form

$$f(X_{F_i}, F_i, X_{B_i}, B_i) = 1 - (X_{F_i} F_i)/(X_{B_i} B_i)$$

Convergence of Newton's method is dependent on the initial guess, therefore, linear profiles are used for the flow rates, brine temperature, heat transfer area, and the ratio α. The guess for the steam flow rate is based on the approximate relation of the number of effects and the performance ratio.

4.3.3 System Performance

Performance of the two MEE systems is analyzed as a function of the intake seawater salinity, number of effects, and the top brine temperature. Performance parameters include the thermal performance ratio, the specific cooling water flow rate, conversion ratio, and the specific heat transfer area. Also, analysis is presented for the dependence of the heat transfer area for evaporation and brine heating on the system operating conditions. Finally, comparison is made between model predictions and the forward feed MEE and MSF systems.

Figure 12 shows the performance of the MEE parallel feed as function of the heating steam temperature and the seawater salinity. As is shown the decrease in thermal performance ratio decreases at higher heating steam temperature is caused by three factors, which includes:
- Increase in the amount of sensible heat required for increasing the temperature of the feed seawater to higher boiling temperatures, since the feed temperature (T_f) is kept constant at 35 °C.

- Increase in the amount of feed flow rate because of decrease in the conversion ratio.
- Decrease in the latent heat of the heating stream at higher temperatures.
- These factors result in the consumption of larger amount of steam and consequently reduction in the thermal performance ratio. Increase in the heating steam temperature reduces the specific heat transfer area due to the increase in the temperature drop per stage, which enlarges the driving force for heat transfer. Also, at higher temperatures the value of the overall heat transfer coefficient augments causing the decrease in the heat transfer area. Another effect is caused by the increase in the brine salinity at low temperatures, which results in an increase of the boiling point elevation. This lowers the vapor temperature and consequently the driving force for heat transfer. Therefore, at lower heating steam temperatures the area for heat transfer increases drastically. At higher temperatures, the decrease in the amount of the specific cooling water is associated with the increase in the amount of feed flow rate, which is caused by reduction in the conversion ratio. The decrease in the conversion ratio at higher top brine temperature is caused by the limitations imposed by the maximum salinity of the rejected brine.

Effects of the seawater salinity on the system performance are also shown in Fig. 12. As is shown larger differences in the performance ratio, the specific cooling seawater, and the conversion ratio are obtained at higher heating steam temperatures. This is caused by the decrease in the limit imposed on the salinity of the rejected brine, which results in large decrease of the conversion ratio and the subsequent increase in the feed flow rate. Combining Eqs. (1 and 2) can easily prove reduction in the amount of vapor formed per stage upon increase of the seawater salinity. The resulting relation, $D_i/F_i = (X_{B_i}-X_{F_i})/X_{B_i}$, show that increasing X_{F_i} at constant temperature (which implies constant X_{B_i}) would reduce the ratio on the right hand side of the equation and consequently the amount of vapor formed. As a result, the system thermal performance ratio, specific cooling water flow rate, and conversion ratio decreases at higher seawater salinity. As is shown, the specific heat transfer area is insensitive to changes in the seawater salinity, since it only depends on the thermal load, the heating steam temperature, the temperature drop per stage, and the overall heat transfer coefficient.

Results for increasing the number of effects for the MEE parallel feed are shown in Fig. 13. As is shown, increasing the number of effects gives higher thermal performance ratios and larger specific heat transfer areas. The increase in the specific heat transfer area is caused by reduction in the driving force for heat transfer, or the temperature drop per stage. This is because the heating steam temperature and the brine temperature in the last effect are kept constant. The increase in the system performance ratio for larger number of effects is a result of increasing the number of vapor reuse in the system. In the

first effect, the latent heat of the heating steam is used to heat the feed seawater to the saturation temperature and to form a smaller amount of vapor. This process is repeated in subsequent effects, where the feed seawater is heated and an additional amount of vapor is formed. The decrease in the specific cooling water flow rate for larger number of effects is caused by the reduction in the amount of vapor formed per effect. The decrease in the conversion ratio is also caused by limits imposed on the maximum salinity of the rejected brine. As is shown in Fig. 13, operation of the 8-effect system in parallel mode is limited to a minimum heating steam temperature of 70 °C. At lower heating steam temperatures the temperature range for the brine in the first and last effects is small. Therefore, the combined effect of the boiling point elevation and the temperature drop per stage results in a heat transfer pinch, i.e., the vapor temperature in effect i is less than the brine temperature in effect i+1.

Analysis of variations in the heat transfer areas for evaporation and feed heating for the parallel flow system shows high sensitivity to the heating steam temperature and some dependence on the number of effects. For example, at a heating steam temperature of 100 °C and four effects the area for evaporation constitutes 78, 92, 96, and 98% of the total heat transfer area from the first to the last effects, respectively. For a lower heating steam temperature of 70 °C, the evaporation heat transfer area varies over a narrower range of 95 to 98% of the total heat transfer between the first and last effect. Increasing the number of effects increases the range over which the evaporation heat transfer area varies. For example, in the 8-effect system and at a heating steam temperature of 100 °C the evaporation heat transfer area varies over a wider range of 68 to 99% between the first and the eighth effects. From the above, it can be seen that the heat transfer area for evaporation is lower at higher heating steam temperatures. This is because of the increase in the amount of sensible heat required to increase the temperature of the feed seawater to the saturation temperature.

The performance of the MEE parallel/cross flow system differs from the MEE parallel flow system in the conversion ratio and the specific cooling water flow rate. On the other hand, variations in the thermal performance ratio and the specific heat transfer area for the two systems are similar. As is shown in Figs. 14 and 15, the system conversion ratio remains constant as the heating steam temperature increases. However, the conversion ratio increases at lower salinity for the feed seawater. For this system, the conversion ratio is independent of the heating steam temperature because the salinity of the brine leaving the last effect is defined at the same temperature, which is equal to 40 °C. Therefore, the total mass and salt balance of the system is defined by the relations ($M_F = M_B+M_D$) and ($M_F\ X_F = M_B\ X_B$), which combines to ($M_D/M_F = (X_B-X_F)/X_B$). Accordingly, the conversion ratio is independent of the heating steam temperature, since X_B and X_F are independent of the heating steam temperature. The same conclusion applies to variations in the conversion ratio as a function in

the number of effects, Fig. 15. As is shown the conversion ratio is independent of the number of effects. This is cleared by inspection of the above relation, where the conversion ratio depends only on X_B and X_F. In this regard, X_B is a function of the brine temperature in the last effect, 40 °C, and X_F is an independent parameter. The small increase in the amount of cooling seawater at higher heating steam temperatures and seawater salinity is caused by the decrease in the system thermal performance ratio at higher heating steam temperatures, which implies increase in the specific thermal energy of the system.

Comparison of the parallel feed and the parallel/cross flow systems for n = 4, is shown in Fig. 16, which contains two sets of data for each system. The first set limits the maximum brine concentration to 95% of the $CaSO_4$ solubility limit and the second set has a maximum limit of 70,000 ppm. As is shown, the two systems have similar variations in the thermal performance ratio and the specific heat transfer area, where both parameters decrease at higher heating steam temperature. Differences among the two systems are found upon comparison of the specific cooling water flow rate and the conversion ratio. Selection among the four operating conditions show that the parallel/cross flow system with a salinity limit of 70000 ppm has the lowest specific flow rate for the cooling seawater, highest thermal performance ratio, and lowest specific heat transfer area. On the other hand, the highest conversion ratio is obtained for the parallel/cross flow system with a salinity limit set by the $CaSO_4$ solubility.

Comparison of the forward and parallel/cross feed systems is shown in Fig. 17. The data for the forward feed system is extracted from a previous study by El-Dessouky et al. (1998). The data for the forward feed MEE and the parallel/cross flow systems are obtained for 12 effects, feed salinity of 42000 ppm, rejected brine salinity of 70000 ppm, intake seawater temperature of 25 °C, feed seawater temperature of 35 °C, and rejected brine temperature of 40 °C. As is shown, the parallel/cross feed has higher specific heat transfer area than the forward feed system, especially at lower top brine temperatures. This is because of the lower driving force for heat transfer, which is manifested in the parallel/cross flow system due to heating of the feed seawater in each from the intake temperature to the saturation temperature. The performance ratio for both systems is almost independent of the heating steam temperature. Also, the performance ratio for the parallel/cross flow system is higher because it is not necessary to heat all the feed to the top brine temperature.

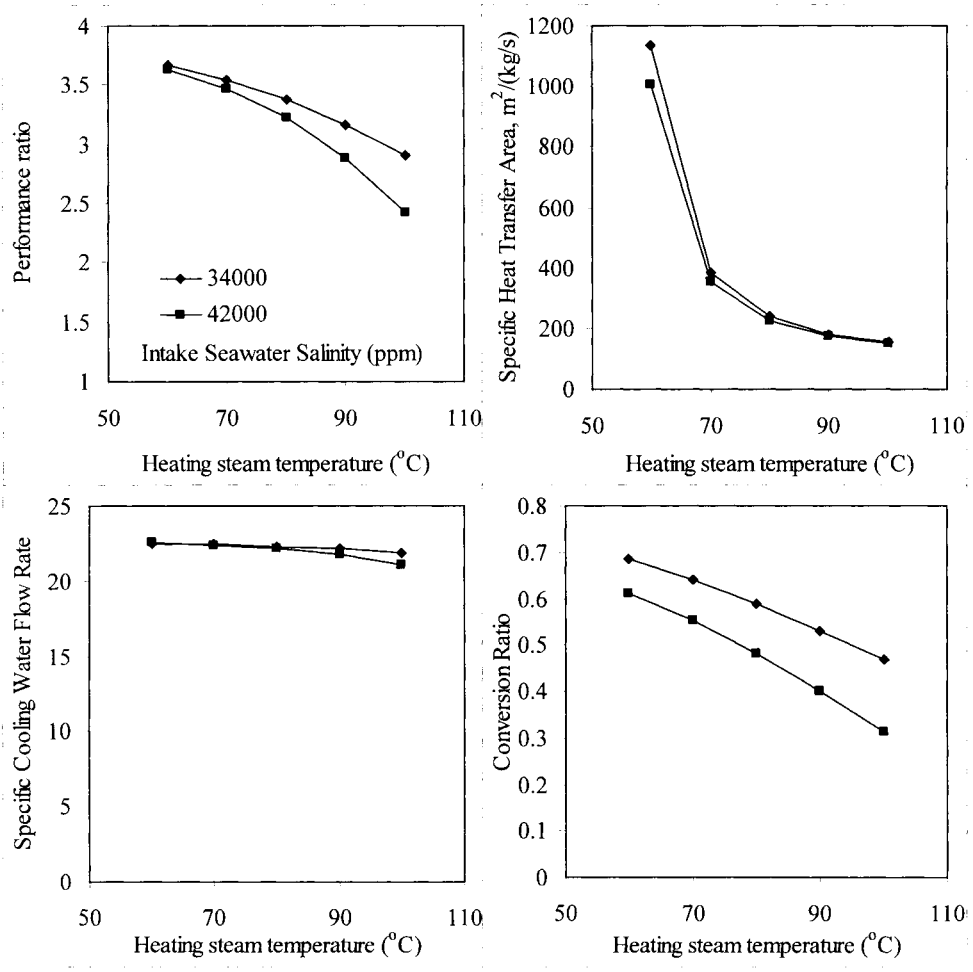

Fig. 12. Dependence of MEE parallel flow system on the heating steam temperature and seawater salinity for n = 4

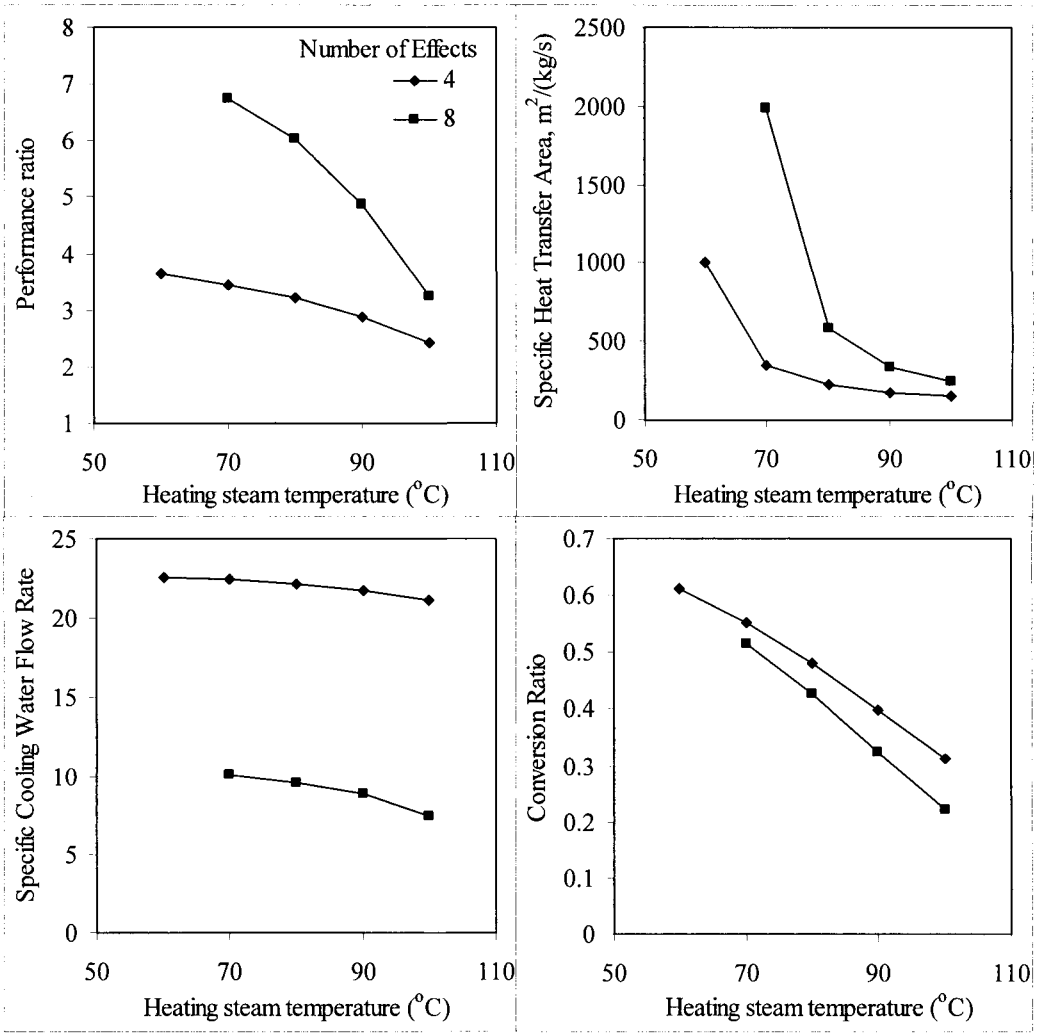

Fig. 13. Dependence of MEE parallel flow system on the heating steam temperature and number of effects for seawater salinity = 42000 ppm

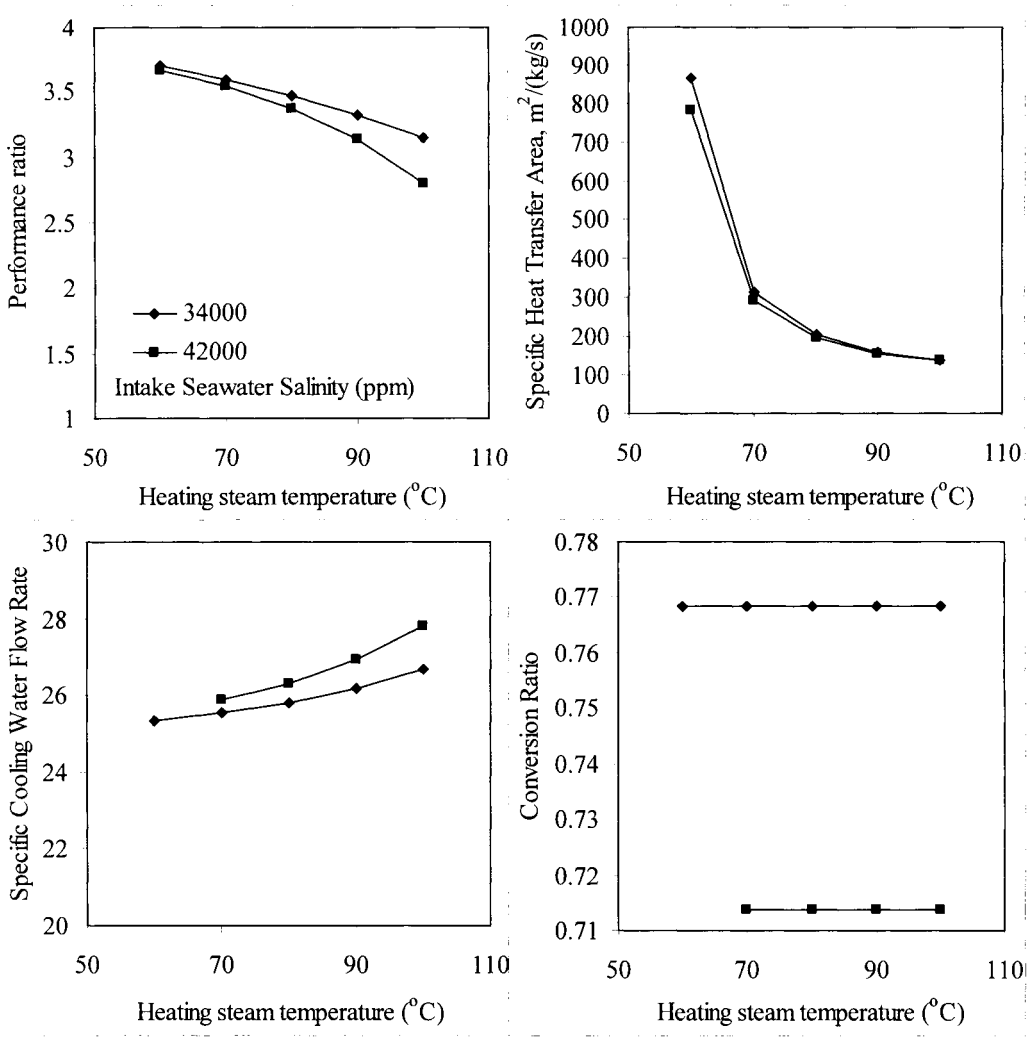

Fig. 14. Dependence of MEE parallel/cross flow system on the heating steam temperature and seawater salinity for n = 4

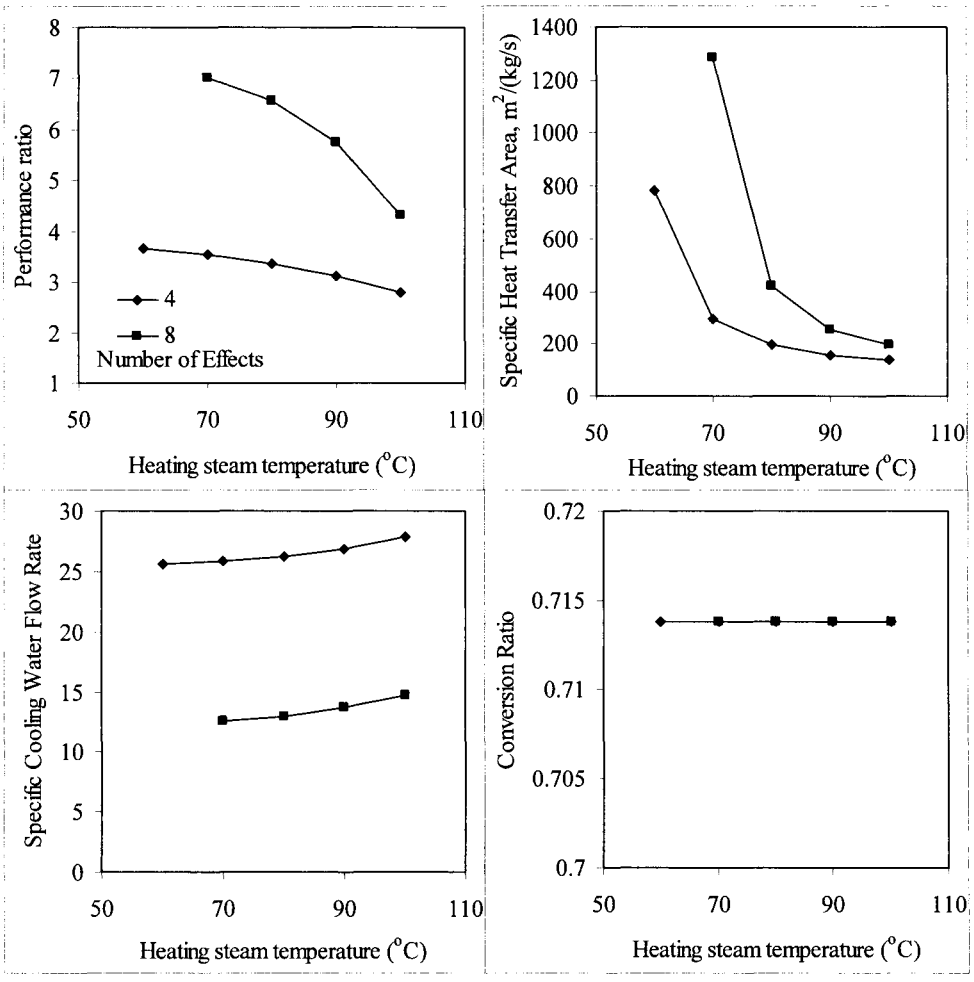

Fig. 15. Dependence of MEE parallel/cross flow system on the heating steam temperature and number of effects for seawater salinity = 42000 ppm

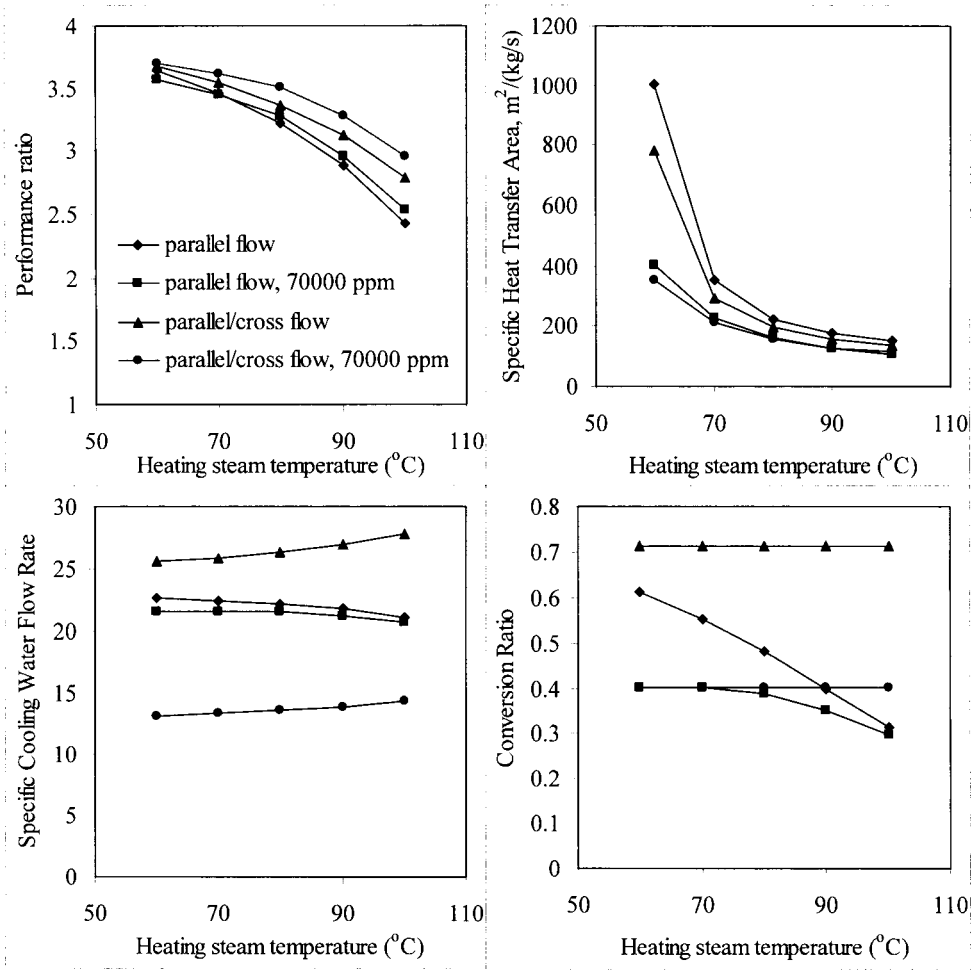

Fig. 16. Comparison of four MEE parallel configurations for n = 4 and seawater salinity = 42000 ppm

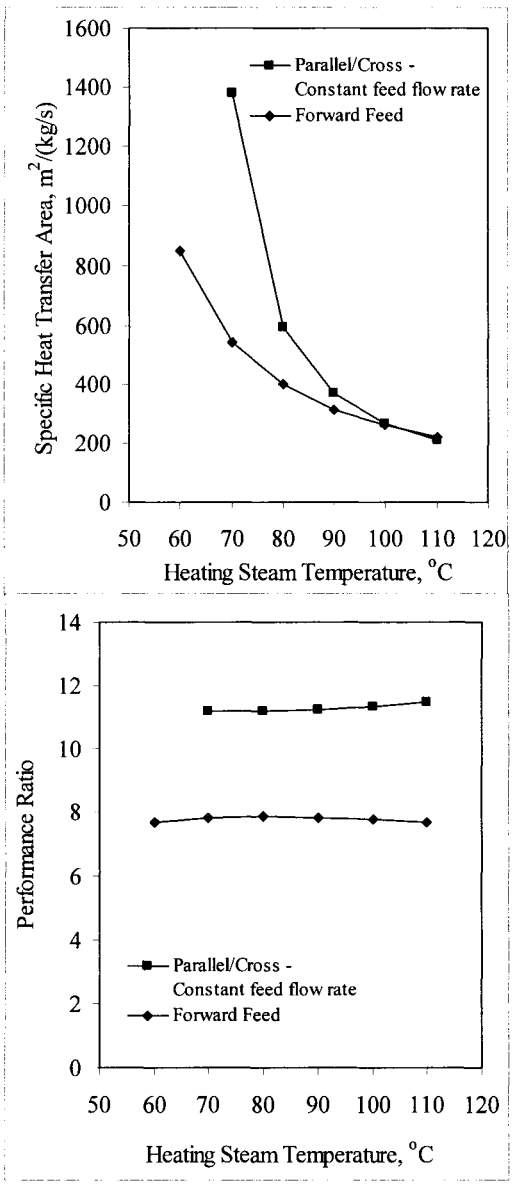

Fig. 17. Comparison of forward and parallel feed MEE for n = 12

4.3.4 Industrial Data and Practice

Comparing the performance of the parallel feed, the forward feed, and the conventional multistage flash system (MSF) is shown in Table 2. As is shown the performance ratio for the MSF system with 24 stages is 8, while the performance ratio for the MEE configurations with 8 effects varies from 4.9 to 5.2, and the 12 effect systems have an average value of 8. The specific heat transfer area for the MEE systems vary over a range of 200-500 $m^2/(kg/s)$ as the number of effects is increased from 8 to 12. As for the specific heat transfer area for the MSF system it has a value of 275 $m^2/(kg/s)$. It should be noted that the MEE forward feed system is not found on commercial scale and is limited to the conceptual design presented here.

Table 2: Comparison of MSF, forward feed MEE, parallel/cross flow MEE for intake seawater salinity of 42,000 ppm, heating steam temperature of 90 °C.

	MSF El-Dessouky et al. (1995)	MEE Forward feed El-Dessouky et al. (1998)	MEE Parallel	MEE Parallel Cross
Number of effects/stages	24	8	8	8
Performance Ratio	8	5.2	4.9	5.8
Specific heat transfer area	259	212	335	255
Conversion ratio	0.4	0.4	0.325	0.714
Salinity of rejected brine	70000	70000	62247	146776
Specific flow rate of cooling water	2.4	2.6	8.9	13.7
Specific pumping power	8.3	4.12	7.78	9.85

4.3.5 Summary

Performance analysis of various configurations shows that the best performance is obtained for the parallel/cross flow MEE. However, the parallel flow system has similar performance characteristics; moreover, its design, construction, and operation is simpler. Operation of both systems is favored at higher temperatures because of the drastic reduction in the specific heat transfer area. However, operation at lower temperatures gives higher thermal performance ratio and lower specific flow rate of the cooling water. Final selection of the most efficient and least expensive system and operating

conditions necessitate full system optimization. The developed models should prove to be highly valuable in selecting and determining the characteristics of the optimum system.

Comparison of the MSF, forward feed, parallel, and parallel/cross flow MEE systems show several advantages of the forward feed MEE over the other systems. It is certain that the engineering design of the forward feed MEE is more energy efficient since it has the lowest specific power consumption, specific heat transfer area, and specific cooling water flow rate. Advantages of the forward feed MEE over the MSF system are found in the lower number of effects and specific power consumption. The forward feed and parallel flow MEE systems have similar or higher thermal performance ratio than the MSF system, however, the number of effects is only 12 for the MEE systems, while it is equal to 24 stages in the MSF system. Also, the MSF system has higher specific power consumption, which is required for pumping the brine circulation stream.

References

El-Dessouky, H.T., Shaban, H.I., and Al-Ramadan, H., Steady-state analysis of multi-stage flash desalination process, Desalination, **103**(1995)271-287.

El-Dessouky, H.T., Alatiqi, I., Bingulac, S., and Ettouney, Steady- H.M., state analysis of the multiple effect evaporation desalination process, Chem. Eng. Technol., **21**(1998)15-29.

Miyatake, O., Murakami, K., Kawata, Y., and Fujii, Fundamental Experiments with Flash Evaporation, Heat Transfer Jpn. Res., **2**(1973)89-100.

This Page Intentionally Left Blank

This Page Intentionally Left Blank

Chapter 5

Multiple Effect Evaporation Vapor Compression

Objectives

The objective of this chapter is to analyze and evaluate the performance of the multiple effect evaporation systems combined with various types of heat pumps. The analysis includes performance of the following systems:

- Parallel feed multiple effect evaporation with thermal or mechanical vapor compression heat pumps.
- Forward feed multiple effect evaporation with thermal, mechanical, absorption, or adsorption vapor compression heat pumps.

The performance of the parallel feed systems is compared against industrial data. However, the forward feed system presents only results of the system design, since there are no industrial units for these systems.

5.1 Parallel Feed Multiple Effect Evaporation with thermal and mechanical vapor compression

The parallel feed multiple effect evaporation is the industrial standard for seawater desalination using the multiple effect evaporation process. The parallel feed configuration has several attractive features including simple process layout, stable and wide operating range. The process model and performance has similar features to the forward feed configuration. The following sections include models and analysis for the thermal and mechanical vapor compression processes of the parallel and parallel/cross flow configurations.

As discussed in previous sections, the MEE-MVC system is thought to increase the system capacity. As will be shown later, use of this configuration has no effect on the specific power consumption. The market share of the MEE-MVC is less than 1%. On the other hand, the MEE-TVC has a higher share close to 5%. Both processes have attractive features that make them highly competitive against other well-established desalination processes that include the MSF and RO.

Limited number of field studies can be found on the MEE-TVC system, which include the following:

- Michels (1993) reported a number of outstanding features for the MEE process when combined with thermal vapor compression (MEE-TVC). These features include low corrosion and scaling, which is caused by low temperature operation (top brine temperature below 60°C). Other features include low energy consumption, short delivery time, easy operation and maintenance, proven reliability in the Gulf region. The cost of the plant erection, civil work, and the seawater intake is 35% cheaper than the MSF plants. Michels (1993) described three low capacity units of MEE with thermal vapor compression built in the remote western areas of the Emirate

of Abu Dhabi, UAE. The plants superseded the more classic multi stage flash (MSF) in the range of unit productions up to about $10x10^3$ ton/day.

- Temstet and Laborie (1996) outlined the main characteristic of a dual-purpose multi-effect desalination plant. The system is designed to switch automatically between two operating modes, which depends on the seasonal variations in power and water demand. The first mode combines the MEE system with a single-stage steam jet ejector, which compresses the vapor extracted from the last effect. The second mode of operation involves the use of low pressure heating steam. The plant operates over a low temperature ranges, includes 12 effects, and has a production capacity of 12000 m^3/day.

Other studies of the MEE-TVC system focus on modeling and performance evaluation. Examples for these studies include the following:

- Minnich et al. (1995) developed a simple model for the MEE-TVC system. The MEE system operates at low temperatures and in the parallel mode. The model is used to compare the performance and capital cost of the MEE-TVC versus the MSF and MEE systems. The capital cost for the three systems is based on the total heat transfer area. Several simplifying assumptions are used to develop the model and it includes:
  - Constant and equal temperature losses in all effects,
  - Constant and equal overall heat transfer coefficients in all effects,
  - Constant thermal load in all effects,
  - Negligible distillate flashing,
  - No feed preheaters,
  - Equal feed flow rates in all effects,
  - Negligible difference of latent heat and vapor enthalpy,
  - Constant specific heat and vapor enthalpy, and
  - Negligible pressure losses in the system components, demister and connecting tubes.

The model results show that operation of the MEE-TVC system at low top brine temperatures, 60 °C, gives higher heat transfer areas than the MSF system at performance ratios higher than 6. The capital cost the low temperature MEE-TVC system exceeds the MSF at performance ratios higher than 8. Merits of the MEE-TVC are only realized at higher top brine temperatures.

- Darwish and El-Dessouky (1995) developed a simple model for parallel feed MEE-TVC. The model includes balance equations for energy and mass in each effect and in the steam jet ejector. The ejector model is based on the graphical performance data for steam jet ejectors presented by Power (1994). The model assumes negligible pressure losses within the system components, constant and equal boiling point rise in all effects, and constant temperature drop per effect. In addition, the model did not include equations for the heat transfer areas and the distillate flashing boxes. The model is used to analyze a four-effect MEE-TVC system and results gave a performance ratio of 7.65 for a top brine temperature of 62 °C. The simplicity of the model imposes restrictions

on its use for system design or analysis. For example, a constant temperature drop per effect when used to calculations of the heat transfer area would result in varying area in the system effect. This result is the opposite of industrial practice, where constant heat transfer area is used in all effects to reduce construction and maintenance cost.

- El-Dessouky (1997) and El-Dessouky et al. (1998) developed extensive mathematical models for the single effect thermal vapor compression process (TVC) and the multiple effect systems (MEE). The model, results, and analysis for the single-effect TVC and the stand alone MEE form the basis for development of the more complex MEE-TVC model. Development of both models addressed the limitations found in previous literature studies. Discussion and details of the MEE system are presented in the previous chapter. As for the TVC model, it includes analysis of the evaporator/condenser and the steam jet ejector units. The model includes the energy and material balance equations for the evaporator/condenser, the ejector design equation, the heat transfer design equation for the evaporator/condenser, and correlations for the heat transfer coefficient, thermophysical properties, and thermodynamic losses. Predictions show that the performance ratio varies between 1 and 2 as the top brine temperature is increased from 60 to 100 °C. The performance ratio increases as the pressure of the motive steam is increased. This makes the motive steam capable of compressing larger amounts of the entrained vapor. As a result, the amount of motive steam is reduced causing the increase of the performance ratio. The system performance ratio is found to increase at lower compression ratios (pressure of compressed vapor/pressure of entrained vapor). At low compression ratios, the amount of motive steam required to compress the entrained vapor are smaller and as a result the system performance ratio increases. Lower heat transfer areas for the evaporator condenser are predicted at higher top brine temperatures, because of the increase in the overall heat transfer coefficient at higher temperatures. The specific flow rate of cooling water is found to decrease as the amount of entrained vapor to the steam ejector is increased. The behavior occurs at high top brine temperature, low motive steam pressures, and high compression ratios.
- El-Dessouky and Ettouney (1997) presented analysis of the MEE-TVC system. The developed MEE-TVC model is based on the two models developed by El-Dessouky (1997) for the single-effect TVC and the multiple effect MEE model developed by El-Dessouky et al. (1998). As a result, the MEE-TVC model is based on sound physical phenomena, which relates various processes occurring in the system. The model results show large increase in the system performance ratio over the stand alone MEE system, with increase varying from 20-50%. In addition, large reduction is obtained in the specific flow rate of cooling water.

5.1.1 Process Description

Figs. 1a and 1b show the MEE-P/TVC and MEE-PC/MVC processes. As is shown both systems include n effects and n-1 flashing boxes. Each effect includes a vapor space, demister, condenser/evaporator tubes, brine spray nozzles, and brine pool. In either system, the effects are numbered 1 to n from the left to right (the direction of the heat flow). Vapor flows from left to right, in the direction of falling pressure, while the feed seawater flows in a perpendicular direction. Compressed vapor is introduced into the tube side in the first effect; while, on the shell side feed seawater is sprayed on the tubes top rows. The brine spray forms a thin falling film on the succeeding rows within the evaporator. In the first effect, the brine falling film absorbs the latent heat of the compressed vapor. As a result, the brine temperature increases to saturation, where, evaporation commences and a smaller amount of vapor forms. This vapor is used to heat the second effect, where, it condenses on the tube side and releases its latent heat to the brine falling film. This process is repeated for all effects, until effect n.

In both systems, the condensed vapor in effects to 2 to n is introduced into the associated flashing box, where the temperature of the condensed vapor is reduced through flashing of a small amount of vapor. The flashed off vapor is routed into the tube side of the next effect together with the vapor formed by boiling or flashing within the previous effect.

In the MEE-P/TVC system, the vapor formed in the last effect is introduced into the down condenser. A controlled amount of intake seawater is routed into the tube side of the down condenser, where it condenses part of the vapor formed in the last effect. The steam jet ejector entrains the remaining part of the vapor, where it is compressed by the motive steam to the desired pressure and temperature. The warm intake seawater stream leaving the down condenser is divided into two parts; the first is the feed seawater stream, which is distributed among the evaporation effects, and the second is the cooling seawater stream, which is reject back to the sea. The cooling seawater stream removes the heat added to the system by the motive steam.

In the converging section of the steam jet ejector the kinetic energy of the motive steam increases drastically and its speed becomes supersonic near the contraction point. Consequently, its pressure drops to low values and allows for suction of the entrained vapor. Mixing of the motive steam and the entrained vapor takes place past the ejector contraction. In the diverging section, the mixture velocity is reduced, while, its pressure starts to increase. The compression process is controlled by the ejector geometry and the motive steam properties.

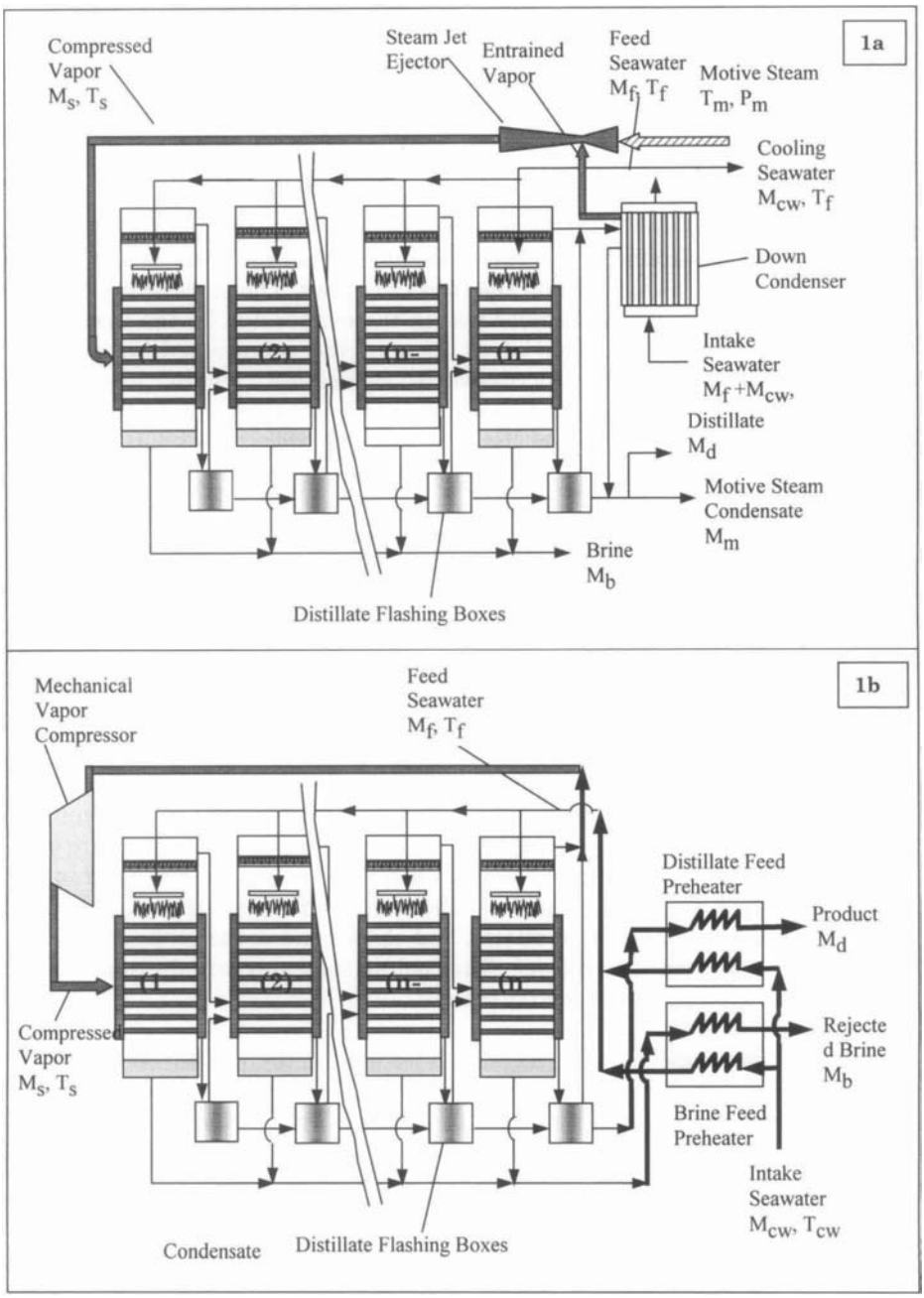

Fig. 1. Schematic of multiple effect evaporation with vapor compression(1a: parallel feed thermal vapor compression, MEE-P/TVC) and (1b: Parallel feed mechanical vapor compression, MEE-P/MVC).

The mechanical vapor compression system is distinguished by absence of the down condenser and use of the feed preheaters. Removal of the down condenser is a result of routing the entire vapor formed in the last effect to the mechanical vapor compressor, where the vapor is superheated to the desired temperature and pressure. At the other end, the feed preheaters recover part of the sensible heat found in the rejected brine and distillate product streams. This improves the system thermal efficiency and maintains production at the design levels, especially, during winter operation.

The main difference of the MEE-P and MEE-PC is that in the later system, the brine leaving effect (i) is introduced into the brine pool of effect (i+1). As a result of the positive temperature difference for the brine of effects (i) and (i+1), a small portion of the feed brine flashes off as it is introduced into effect (i+1). The flashed off vapors improves the system productivity and thermal efficiency. In effect (i+1), the flashed off vapors are added to the vapor formed by boiling within the same effect. As for the MEE-P process, the brine leaving each stage is directly rejected to the sea.

5.1.2 Process Modeling

Similarities among various systems considered in this analysis necessitate simultaneous development of the balance equations for various components within each system. Common assumptions among various models include steady state operation, constant heat transfer area in each effect, negligible heat losses to the surroundings, and salt free distillate product.

The following sections include discussion of the model equations for various components within the MEE-PC system. The model equations for the MEE-P system are not given, because of the similarity with the MEE-PC system. However, the discussion points to differences in balance equations of the MEE-P system. As for the correlations used to calculate the thermodynamic losses, pressure drops, and physical properties are given in the appendix. Fig. 2 shows a schematic for the system variables in the evaporator and the associated flash box in effect i. The figure includes flow rates, salinity, and temperatures of various streams as it enters and leaves the evaporator and the flashing box.

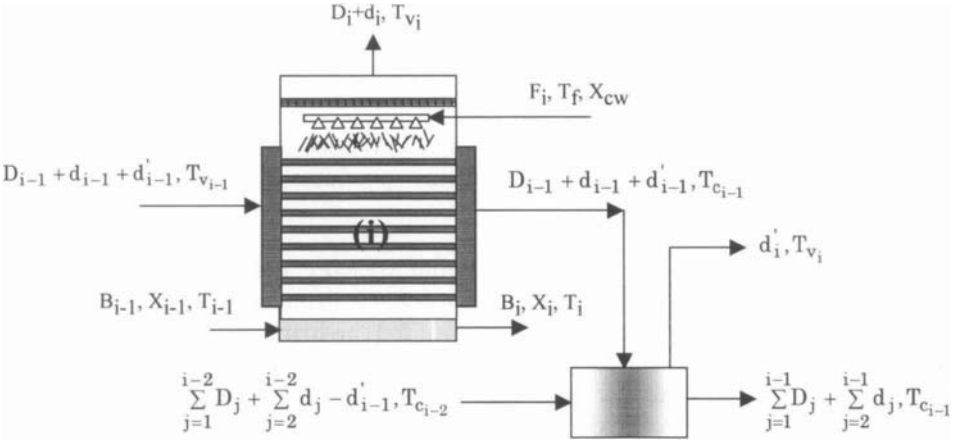

Fig. 2. Variables in evaporator and flash box of effect i.

Balance Equations for Each Effect

The mathematical model for each effect includes the material and energy balances as well as the heat transfer equation. The model includes the following equations:

- Total balance in effect i

$$F_i + B_{i-1} = D_i + B_i \tag{1}$$

- Salt balance in effect i

$$X_{F_i} F_i + X_{B_{i-1}} B_{i-1} = X_{B_i} B_i \tag{2}$$

In Eqs. 1 and 2, B, D, and F are the flow rates of brine, distillate, and feed, X is the salinity, and the subscripts B, F, and i designate the brine, feed, and the effect number.

- Rejected brine salinity

$$X_b = 0.9(457628.5–11304.11T_b+107.5781T_b^2–0.360747T_b^3) \tag{3}$$

This equation is used to calculate the reject brine salinity in each effect as a function of the brine temperature. This equation is obtained by curve fitting of the salinity/temperature relation for the solubility 90% of the solubility of $CaSO_4$. The upper limit on the rejected brine salinity is set at 70,000 ppm.

- Energy balance for effect i

$$D_{i-1}\,\lambda_{i-1} + d_{i-1}\,\lambda_{i-1} + d'_{i-1}\,\lambda'_{i-1} = F_i\,C_p(T_i - T_f) + D_i\lambda_i \quad (4)$$

In the above equation d is the amount of vapor formed by brine flashing in effect i-1, d' is the amount of vapor formed by flashing in the flashing boxes, λ is the latent, C_p is the specific heat at constant pressure, T_i is the brine boiling temperature, and T_f is the feed seawater temperature. In Eq. (4) the first term corresponds to the heat added to the effect by condensing the vapor generated in the previous effect. This only applies to effects 2 to n, since heating steam from an external source is used to drive the system and heat the first effect. In effect 3 to n, the second term in Eq. (4) defines the amount of heat associated with condensation of the vapor formed by brine flashing in the previous effect. The third term, which applies only to effects 3 to n, corresponds to the heat added to the effect by condensing the vapor generated in the distillate flashing box associated with the previous effect. The fourth term in Eq. 4 gives the amount of heat gained by the feed stream, where its temperature increased inside the effect from the seawater temperature to the brine boiling temperature. The last term gives the amount of heat consumed by the vapor generated inside the effect. In the above equation the specific heat at constant pressure depends on the brine salinity and temperature, while the latent heat depends on the vapor temperature. Correlations for the two properties are given in the appendix.

- Vapor temperature in effect i

$$T_{vi} = T_i - BPE_i \quad (5)$$

where BPE is the boiling point elevation and T_v is the vapor temperature.

- The vapor condensation temperature

$$T_{ci} = T_i - BPE_i - \Delta T_p - \Delta T_t - \Delta T_c \quad (6)$$

In Eq. 5, the condensation temperature, T_{ci}, is lower than the brine boiling temperature, T_i, by the boiling point elevation and the losses caused by pressure depression in the demister (ΔT_p), friction in the transmission line (ΔT_t), and during condensation (ΔT_c).

- Amount of vapor formed by brine flashing inside the effect

$$d_i = B_{i-1}\,Cp\,\frac{T_{i-1} - T'_i}{\lambda_i} \quad (7)$$

with

$$T'_i = T_i + NEA_i \quad (8)$$

In Eq. 7, T_i' is the temperature to which the brine cools down as it enters the effect. Also, the latent heat λ_i is calculated at the effect vapor temperature, T_{v_i}. The term $(NEA)_i$ is the non-equilibrium allowance and is calculated from the correlation developed by Miyatake (1973):

$$(NEA)_i = \frac{33.0\,(T_{i-1} - T_i)^{0.55}}{T_{v_i}}$$

– Amount of vapor flashed off in the distillate flashing boxes

$$d_i' = D_{i-1} C_p \frac{(T_{c_{i-1}} - T_i'')}{\lambda_i'} \tag{9}$$

with

$$T_i'' = T_{v_i} + (NEA)_i$$

where $(NEA)_i$ is the non-equilibrium allowance and is equal to $(NEA)_i = 0.33\frac{(T_{c_{i-1}} - T_{v_i})}{T_{v_i}}$, T_i'' is the temperature to which the condensing vapor cools down to as it enters the flashing box.

– Heat transfer area in effect i

$$D_{i-1}\,\lambda_{i-1} + d_{i-1}\,\lambda_{i-1} + d_{i-1}'\,\lambda_{i-1}' = F_i\,C_p(T_i - T_f) + D_i\lambda_i$$
$$= A_{1i}\,U_{1i}\,(LMTD)_i + A_{2i}\,U_{2i}\,(T_{c_i} - T_i) \tag{10}$$

$$\alpha(D_{i-1}\,\lambda_{i-1} + d_{i-1}\,\lambda_{i-1} + d_{i-1}'\,\lambda_{i-1}') = D_i\lambda_i = A_{2i}\,U_{2i}\,(T_{c_i} - T_i) \tag{11}$$

$$(LMTD)_i = (T_i - T_f)/\ln((T_{c_i} - T_f)/(T_{c_i} - T_i)) \tag{12}$$

where A_{1i} is the heat transfer area for sensible heating of the brine from the feed to the boiling temperature in each effect and A_{2i} is the heat transfer area for evaporation, U_{1i} and U_{2i} are the corresponding overall heat transfer coefficient, LMTD is the logarithmic heat transfer coefficient, and α is the fraction of input heat consumed by vapor formation.

Balance Equations for the Down Condenser

The down condenser balance equations include the energy balance and heat transfer rating equation.

- Energy balance of the down condenser

$$(d_n + d'_n + D_n)\lambda_n = (M_{cw} + M_f)\, Cp\, (T_f - T_{cw}) \tag{13}$$

- Rating of the down condenser

$$(d_n + d'_n + D_n)\lambda_n = U_c\, A_c\, (LMTD)_c \tag{14}$$

$$(LMTD)_c = (T_f - T_{cw})/\ln((T_{v_n} - T_{cw})/(T_{c_n} - T_f)) \tag{15}$$

where A_c, U_c, and $(LMTD)_c$ are the heat transfer area, overall heat transfer coefficient, and logarithmic mean temperature difference.

In presence of the steam jet ejector, the thermal load of the down condenser is lower since the part of the vapor formed in the last effect and the associated flashing box is entrained in the steam jet ejector. Therefore, the vapor formed in the last effect is defined by

$$M_{ev} + M_u = (d_n + d'_n + D_n) \tag{16}$$

where M_{ev} and M_u are the flow rates of the entrained and un-entrained vapor, respectively. In the following section, which includes the steam jet ejector model, the flow rate of the entrained vapor is obtained from the ejector entrainment ratio.

Model of the Steam Jet Ejector

The steam jet ejector is modeled by the semi-empirical model developed by El-Dessouky (1997). The model makes use of the field data collected over 35 years by Power (1994) for vapor entrainment and compression ratios of steam jet ejectors. The compression ratio, Cr, is the pressure ratio of the compressed and entrained vapors. The entrainment ratio is flow rate ratio of the motive steam and the entrained vapor. The entrainment ratio, Ra, is calculated from the following relation

$$Ra = 0.296 \frac{(P_s)^{1.19}}{(P_{ev})^{1.04}} \left(\frac{P_m}{P_{ev}}\right)^{0.015} \left(\frac{PCF}{TCF}\right) \tag{17}$$

where, P_m, P_s and P_{ev} are the pressures of the motive steam, compressed vapor, and entrained vapor respectively, PCF is the motive steam pressure correction factor and TCF is the entrained vapor temperature correction factor. The following two equations are used to calculate PCF and TCF

$$PCF = 3x10^{-7} (P_m)^2 - 0.0009 (P_m) + 1.6101 \quad (18)$$

$$TCF = 2x10^{-8} (T_{ev})^2 - 0.0006 (T_{ev}) + 1.0047 \quad (19)$$

where P_m is in kPa and T_{ev} is in °C. The previous equations are valid only for ejectors operating with steam as the motive fluid and the entrained gas is water vapor. These equations are valid in the following ranges: $Ra \leq 4$, $500 \geq T_{ev} > 10$ °C, $3500 \geq P_m \geq 100$ kPa, and $6 \geq Cr = \frac{P_s}{P_{ev}} \geq 1.81$.

The steam jet ejector must be designed and operated at critical conditions to allow normal and stable operation. This condition is associated with absence of violent fluctuations in the suction pressure. If the ejector is designed to operate with a full stable range, it will have a constant mass flow rate of the entrained vapor for different discharge pressures when the upstream conditions remain constant. The ejector is critical when the compression ratio is greater than or equal to the critical pressure ratio of the suction vapor. For water vapor this ratio is 1.81. That is, the suction pressure must be less than 0.55 times the discharge pressure to obtain critical or stable conditions in the steam jet ejector. The above limit on the compression ratio necessitates the use of two steam jet ejectors in series, Fig. 3, for a wide compression range. For example, in a single jet ejector that compresses a vapor to 80 °C and entrains vapor at 38 °C, the compression ratio in 7.14. This compression value requires the use of two ejectors in series, where the compression range is divided over the two ejectors. The corresponding balance equations for two ejectors in series include the following:

$$M_s = M_{s1} + M_{m2} \quad (20)$$

$$M_{s1} = M_{ev} + M_{m1} \quad (21)$$

$$Ra_1 = M_{m1}/M_{ev} \quad (22)$$

$$Ra_2 = M_{m2}/M_{s1} \quad (23)$$

$$Cr_1 = P_{s1}/P_{ev} \quad (24)$$

$$Cr_2 = P_s/P_{s1} \quad (25)$$

where M is the mass flow rate and the subscripts ev, m, s, 1, and 2 define the entrained vapor, the motive steam, the compressed, first and second ejector.

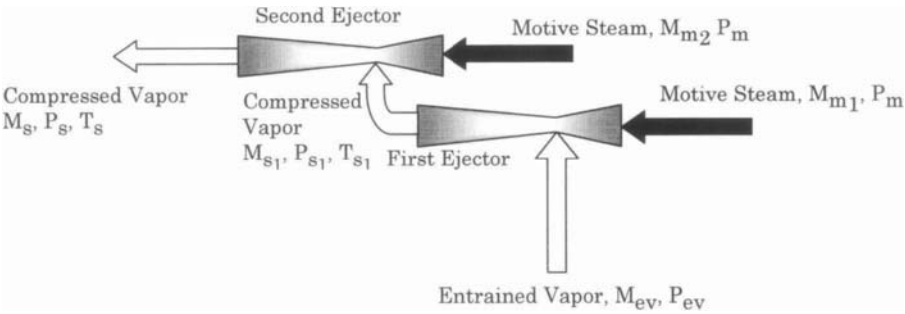

Fig. 3. Schematic of the two ejectors in series.

Model of the Mechanical Vapor Compressor

The specific power consumption of the compressor

$$Q_c = W \rho_d/3600 \tag{26}$$

where ρ_d is the density of distillate product, W is the actual specific work of the compressor, which is given by

$$W = H_s - H_v \tag{27}$$

The enthalpies H_s and H_v are calculated at the compressed vapor temperature, T_s, and the formed vapor temperature in the last effect, T_{vn}, which is lower than $\overline{T}_{vn}$ by the temperature depression caused by pressure drop in the demister. The compressor polytropic specific work is given by

$$\frac{W_m}{W_n} = \eta \left[\frac{(P_s/P_v)^{(\gamma-1/\gamma\eta)} - 1}{(P_s/P_v)^{(\gamma-1/\gamma)} - 1} \right] \tag{28}$$

In Eq. 28 the adiabatic compressibility factor is defined as

$$\gamma = \frac{1}{1 - (1+X)^2 (ZR/Cp_v)/Y} \tag{29}$$

where $X = 0.1846\ (8.36)^{(1/Z)} - 1.539$ and $Y = 0.074\ (6.65)^{(1/Z)} + 0.509$, ASHRAE (1997). In Eq. 29, the compressibility factor Z is set equal 1. The compressor

adiabatic work, W_n, given in Eq. 28 is defined as the enthalpy difference of the in terms of the

$$W_n = H_n - H_v \tag{30}$$

In Eq. 30 H_n and H_v are calculated at T_n and T_{v_n}, respectively, where T_n is calculated from the relation

$$T_n = T_{v_n} (P_v/P_n)^{(\gamma-1)/\gamma} \tag{31}$$

The enthalpy and temperature of the superheated (or compressed vapor) are obtained from the following relations

$$\eta = \frac{W_m}{H_s - H_v} \tag{32}$$

$$H_s = H_d + Cp_v (T_s - T_d) \tag{33}$$

where H_d and T_d are the saturation enthalpy and temperature of the compressed vapor, and H_s and T_s are the superheat enthalpy and temperature of the compressed vapor.

Preheaters Models

Two preheaters are used to increase the intake seawater temperature in the MEE-P/MVC system. This temperature increase is an essential part in energy recovery within the system and it has a strong effect on the plant performance or the specific power consumption. Heating of the feed seawater is performed against the hot product and brine streams leaving the last effect. This process takes place in two plate type heat exchange units, where the intake seawater is divided into two portions, αM_f and $(1-\alpha)M_f$. In the first preheater, heat is exchanged between αM_f and the product water, and in the second preheater, heat is exchanged between $(1-\alpha)M_f$ and the rejected brine. The sum of the thermal load for the two heat exchangers is given in terms of the intake seawater temperature increase. This is

$$Q_h = M_f C_p (T_f - T_{cw}) \tag{34}$$

where Q_h is thermal load of the two preheaters, Cp is the specific heat at constant for the seawater, T_f is feed seawater temperature, and T_{cw} is the intake

seawater temperature. Equation (34) can be also written in terms of the heat load of the product water and the rejected brine, which gives

$$Q_h = M_d\, C_p\, (T_{c_n} - T_o) + M_b\, C_p\, (T_n - T_o) \tag{35}$$

Where T_{c_n} and T_n are the temperatures of the product water and brine leaving the last effect and T_o is the temperature of both streams after leaving the preheaters. Equations 34 and 35 are equated and the result is used to determine the outlet temperature of the heating streams, T_o,

$$M_f\, C_p\, (T_f - T_{cw}) = M_d\, C_p\, (T_{c_n} - T_o) + M_b\, C_p\, (T_{c_n} - T_o) \tag{36}$$

The driving force for heat transfer in the preheaters is taken as the logarithmic mean of the temperature difference at both ends of the preheater. These equations are given by

$$A_d = \frac{M_d C_p (T_{c_n} - T_o)}{U_d (LMTD)_d} = \frac{\alpha M_f C_p (T_f - T_{cw})}{U_d (LMTD)_d} \tag{37}$$

$$\begin{aligned} A_b &= \frac{M_b C_p (T_n - T_o)}{U_b (LMTD)_b} \\ &= \frac{M_d (X_f / (X_b - X_f)) C_p (T_n - T_o)}{U_b (LMTD)_b} \\ &= \frac{(1-\alpha) M_f C_p (T_f - T_{cw})}{U_b (LMTD)_b} \end{aligned} \tag{38}$$

The $(LMTD)_d$ is defined as:

$$(LMTD)_d = \frac{(T_{c_n} - T_f) - (T_o - T_{cw})}{\ln \dfrac{T_{c_n} - T_f}{T_o - T_{cw}}} \tag{39}$$

The $(LMTD)_b$ is defined as:

$$(LMTD)_b = \frac{(T_n - T_f) - (T_o - T_{cw})}{\ln \dfrac{T_n - T_f}{T_o - T_{cw}}} \tag{40}$$

Solution Algorithm

The mathematical models for either system are interlinked and highly nonlinear. Therefore, iterative solution is necessary to calculate the system characteristics. The solution algorithm starts with definition of the following parameters:

- The number of effects varies over a range of 4-12.
- The heating steam temperature varies over a range of 60-100 °C.
- The seawater temperature (T_{cw}) is 25°C.
- The seawater salinity has values of 34,000 ppm or 42,000 ppm.
- The temperature of rejected cooling water or feed seawater (T_f) is less than condensing vapor temperature (T_{c_n}) by 5 °C.
- The boiling temperature in the last effect (T_n) is 40°C.
- The specific heat at constant pressure of the vapor, C_{p_v}, is 1.884 kJ/kg °C.
- The polytropic efficiency of the compressor, η, is 0.76 [24].

The solution algorithm for the thermal vapor compression system is shown in Fig. 4. As is shown, the model equations are solved simultaneously by Newton's method to calculate the following:

- The flow rates, salinity, and temperatures of the feed, brine, and distillate in each effect.
- The heat transfer area for evaporation and sensible heating in each effect.
- The fraction of heat consumed by evaporation in each effect.
- The above results are used to calculate the following:
- The heat transfer area in the condenser.
- The flow rate of cooling seawater.
- The entrainment ratio in the steam jet ejector.
- The amount of motive steam.

Figure 5 shows the solution algorithm for the mechanical vapor compression system. In this system, the amount of compressed vapor is known and is equal to the amount of vapor formed by boiling in the last effect as well as the amount of vapor formed by brine and distillate flashing. The energy and material balance model as well as the compressor model are solved simultaneously and iteratively by Newton's method. Simultaneous solution of the two models gives the following system variables:

- Temperature, salinity, and flow rate profiles of feed, distillate, and brine streams.
- The specific power consumption of the mechanical vapor compressor.
- The temperature of the compressed vapor.
- The heat transfer areas for vapor formation and brine heating in each effect.
- The heat transfer area of the feed preheaters.

The Newton's iterative procedure has an iteration error of $1x10^{-4}$. To facilitate the conversion procedure, each equation is scaled by the largest term found in the equation. Therefore, all equations are in the order of one. For example, the salt balance equation is rearranged into the following form

$$f(X_{cw}, F_i, X_{b_i}, B_i) = 1 - (X_{cw} F_i)/(X_{b_i} B_i)$$

Convergence of Newton's method is dependent on the initial guess, therefore, linear profiles are used for the flow rates, brine temperature, heat transfer areas, and the ratio α. The guess for the steam flow rate is based on the approximate relation of the number of effects and the performance ratio.

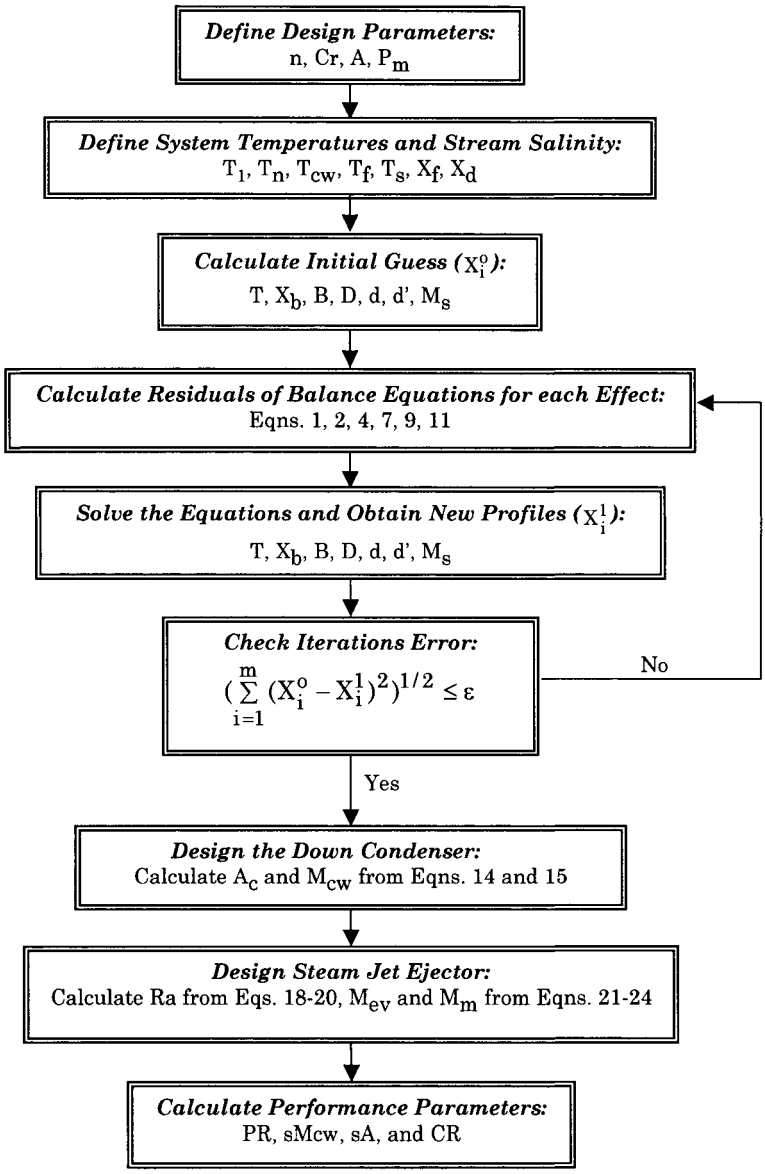

Fig. 4. Solution algorithm of the thermal vapor compression system.

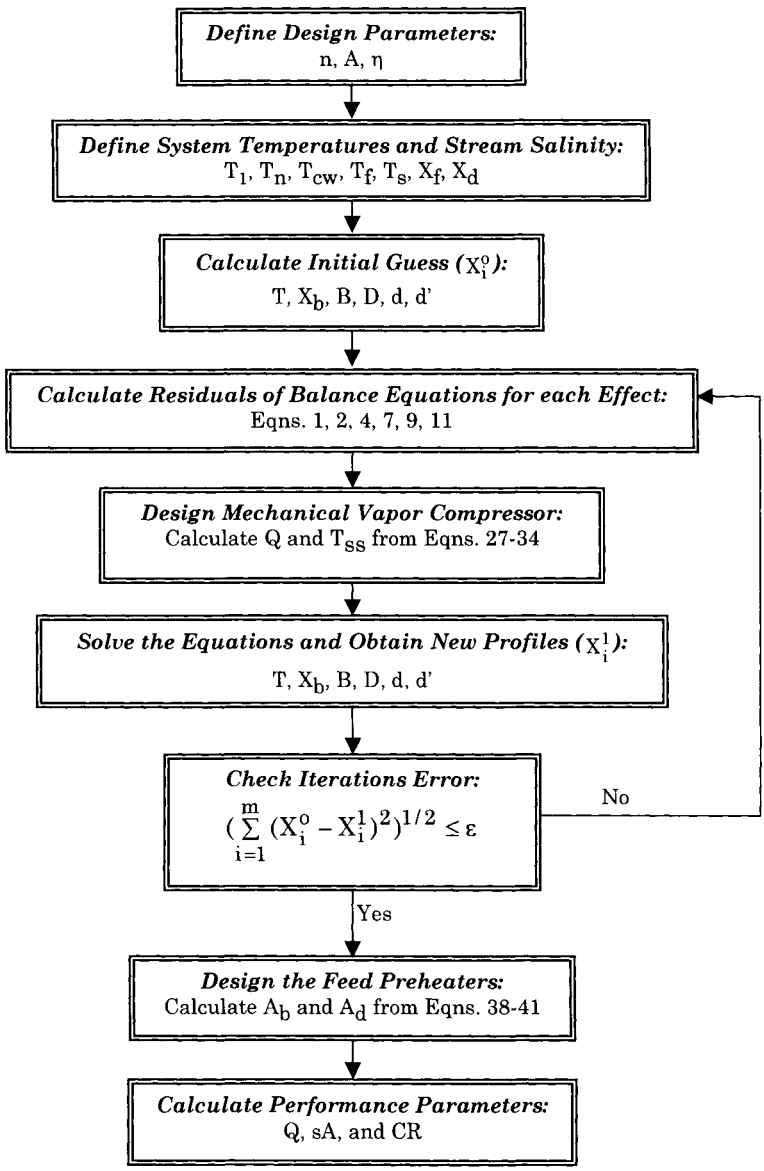

Fig. 5. Solution algorithm of the mechanical vapor compression system.